NGT-36-002-800
GRANT
IN-25
161714
84P.

Electrocatalytic Reduction of Oxygen on Modified Oxide Surfaces

Scott A. Chaffins and Vakula S. Srinivasan
Bowling Green State University
Bowling Green, Ohio

and

Joseph Singer
Lewis Research Center
Cleveland, Ohio

September 1988

NASA

TABLE OF CONTENTS

I. INTRODUCTION

1. HISTORY AND DEVELOPMENT

The hydrogen-oxygen (H_2-O_2) fuel cell was first
reported by Grove [1] in 1839. In his experiments, Grove
described a method in which electricity was generated by
supplying hydrogen and oxygen to two separate electrodes
immersed in sulfuric acid. A schematic diagram of this fuel
cell is given in Figure 1. In the cell hydrogen was
oxidized at the anode, producing hydrogen ions and releasing
electrons into the external circuit. At the cathode,
electrons were accepted from the external circuit, and
oxygen was reduced yielding hydroxide ions (OH^-) [2]. The
net reaction was one in which hydrogen and oxygen combined
to form water.

Since the terminal voltage of an individual fuel cell
is low (approximately one volt) fuel cells are usually
connected in series to provide a more useful output. Such
an arrangement is commonly referred to as a fuel battery.
In 1889, Mond and Langer [2] built a hydrogen-oxygen fuel
battery using electrodes made of platinum sheets covered
with high surface area platinum black separated by a porous
Plaster of Paris diaphragm which contained the electrolyte.
Although the output was poor and the battery expensive, it

1

OXYGEN
CATHODE

$O_2 \longrightarrow O_2$ (ads)

O_2 (ads) + $2H_2O + 4e \longrightarrow 4OH^+$

+

EXTERNAL

CIRCUIT

H_2SO_4

−

HYDROGEN
ANODE

$2H_2 \longrightarrow 2H_2$ (ads)

$2H_2$ (ads) $\longrightarrow 4H^+ + 4e$

NET REACTION
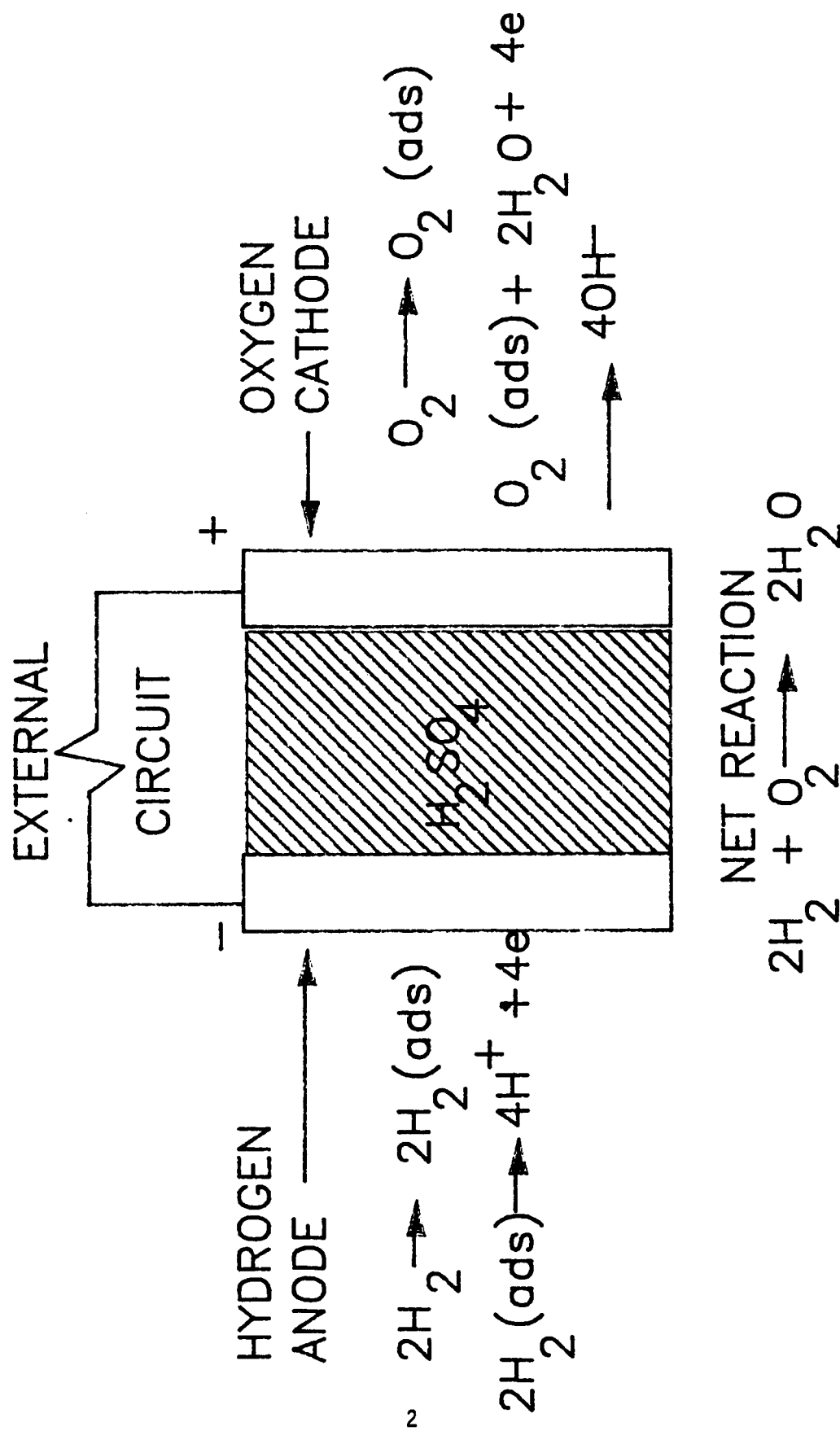
$2H_2 + O_2 \longrightarrow 2H_2O$

Figure 1: Diagram of an acid hydrogen-oxygen fuel cell.

was probably the first fuel battery to give a measurable power [2]. In 1913, Siegl [4] improved the Mond and Langer battery by dispersing the platinum black on carbon particles. The decrease in platinum loading significantly reduced the cost of the fuel cell. In 1965, Haldeman found that greatly enhanced performance could be achieved by mixing a dispersion of Teflon with platinum black catalyst and supporting the resulting mixture on a metal screen.

No real attempts were made to engineer a useful power unit until 1932 when F.T. Bacon and J.C. Frost, working at Cambridge, decided to make a useful power source based on a simple H_2-O_2 cell. Their work culminated in the demonstration of a six kilowatt H_2-O_2 fuel battery [5] in 1959.

As an alternative energy conversion device, fuel cells have shown considerable promise. The most common method of energy conversion is by a heat engine in which heat derived from a chemical reaction is converted to mechanical energy by expanding gases. This process is governed by Carnot's cycle [6], and practical efficiencies for energy conversion are between 30% and 40%. In a fuel cell, fossil fuels like coal can either be oxidized directly, or they can be converted to hydrogen by the water gas process, and the hydrogen oxidized in the fuel cell. Since the efficiency of

3

the fuel cell is not limited by Carnot's cycle, energy
conversion is more efficient than for heat engines, and 75%
practical efficiencies have been demonstrated [7]. Also,
since no combustion takes place, the fuel cells do not
generate pollutants.

Fuel batteries which use phosphoric acid or molten
carbonate electrolyte have been designed for terrestrial use
in utility, commercial, and military applications. One of
the first demonstrations of a fuel battery for commercial
applications came in 1959, when H. K. Ihrig of
Allis-Chalmers demonstrated the now famous 20-horsepower
fuel cell tractor. More recently, United Technology
Corporation has constructed a 4.8 megawatt utility
demonstrator powerplant in Japan [8]. However, fuel
batteries are prohibitively expensive, and few economically
feasible acid fuel cell batteries have been designed for
terrestrial use.

Although terrestrial applications have been limited,
H_2-O_2 fuel batteries have been used in many spacecraft.
An alkaline fuel battery with 1.5 kilowatts of power and
weighing 241 pounds was used as the primary source of
electricity for the NASA Apollo missions [8]. The orbiter
fuel cell power plant, used aboard the NASA Space Shuttle
Orbiter, has an output of 12 kilowatts and weighs 202
pounds. These fuel batteries exhibited power densities
exceeding one watt per square centimeter (W/cm^2) at cell
voltage efficiencies of over 70% [7].

Recently, regenerative H_2-O_2 fuel batteries have been examined as an energy storage device for the NASA Space Station. In this application, solar arrays are used to convert sunlight into electricity during the sunlight portion of the orbit. The excess electricity is used to electrolyze water, producing hydrogen and oxygen gas. These gases are later recombined in the fuel battery during the occult phase of the orbit, generating water and electricity.

2. THE OXYGEN CATHODE

Despite intense efforts [4-7], few commercially viable fuel batteries have emerged. This attests to the difficulties encountered in developing a cost effective fuel battery. A major problem is that, at practical current densities (100 ma/cm^2), cell potentials deviate appreciably from the thermodynamic values. This deviation is primarily due to the irreversibility of the oxygen reduction reactions which take place at the cathode [9]. These reactions are complicated and warrant further discussion.

In an alkaline solution, the electrochemical reduction of oxygen should ideally proceed according to the equation,

$$O_2 + 2H_2O + 4e^- = 4OH^- \quad (1).$$
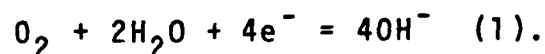
This reaction is predominant on clean platinum [10], iridium [11], rhodium [12], palladium [13], and certain transition metal macrocyclics [14]. One mechanism which has received much support involves the formation and decomposition of
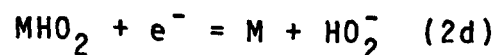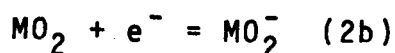
5

surface oxides. The proposed mechanism for the direct four electron reduction of oxygen on platinum is [15],

$$O_2 + 2M = 2MO \quad (1a)$$

$$MO + H_2O + e^- = MOH + OH^- \quad (1b)$$

$$MOH + e^- = M + OH^- \quad (1c).$$
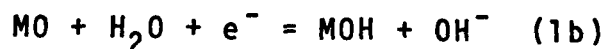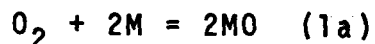
However, studies have shown [10,16-21] that on most surfaces, such as gold [22], mercury [23], and most transition metal macrocyclics like cobalt tetramethoxy phenyl porphyrin (CoTMPP) [24], the electrochemical reduction of oxygen takes place by way of two competing parallel pathways. The first pathway is given by equation (1), and the second pathway is a two electron reduction which is given by the equation,

$$O_2 + H_2O + 2e^- = HO_2^- + OH^- \quad (2)$$
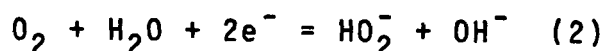
where the perhydroxyl ion (HO_2^-) is formed as a reaction product. Isotope studies carried out by Davies, Clark, Yeager, and Hovorka [25] showed that all of the oxygen in the perhydroxyl ion comes from oxygen gas, and that the O-O bond is not broken during the electrochemical step. One mechanism which is consistent with these findings involves the formation and decomposition of surface oxides. A proposed mechanism for O_2 reduction on Au in an alkaline solution is [15,26],

$$M + O_2 = MO_2 \quad (2a)$$

$$MO_2 + e^- = MO_2^- \quad (2b)$$

$$MO_2^- + H_2O = MHO_2 + OH^- \quad (2c)$$

$$MHO_2 + e^- = M + HO_2^- \quad (2d)$$

6
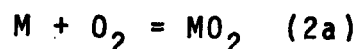
This is only one of several proposed mechanisms [27]. The mechanism may change, depending on parameters such as electrolyte medium, temperature, and electrode material.

It is necessary to reduce the concentration of HO_2^- in order to increase the efficiency of the fuel cell and to prolong electrode life by preventing attack by HO_2^-. This can be accomplished by the further reduction of HO_2^- to OH^-, which forms according to the equation,

$$HO_2^- + H_2O + 2e^- = 3OH^- \quad (3).$$
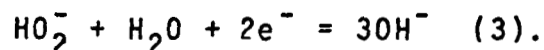
However, this reaction is known to be highly irreversible, and is not expected to contribute significantly to the elimination of HO_2^- [28]. It is also possible to chemically decompose HO_2^- at the electrode surface according to the equation,
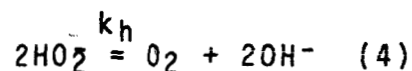
$$2HO_2^- \overset{k_h}{=} O_2 + 2OH^- \quad (4)$$

using a suitable catalyst. This reaction has been found to be first order with respect to the bulk concentration of HO_2^- for a variety of catalysts [29-32]. The oxygen formed as a result of this decomposition can be recycled via reactions (1) and (2), increasing the overall efficiency of the fuel cell. To date no theory of electrocatalysis allows one to predict a priori the activity of a given catalyst, therefore, the development of catalysts for the oxygen electrode has been largely empirical. In the search for a better fuel cell cathode it is necessary to screen catalysts

7

for a high kinetic activity for peroxide decomposition. One of the major goals of the present research is to evaluate five different methods of determining peroxide decomposition rate constants with respect to reliability, and ease of operation. This will be achieved by using powders and Teflon-bonded electrodes of the following catalysts: platinum, gold, CoTMPP, and $La_{.5}Pb_{.5}MnO_3$. Platinum and gold were chosen because they are two of the most intensively studied electrocatalysts for the oxygen cathode. CoTMPP was chosen as a representative of the transition metal macrocyclics because of its performance as an oxygen cathode [9]. $La_{.5}Pb_{.5}MnO_3$ was chosen as a representative of the perovskite class of transition metal oxides as it had the highest activity for peroxide decomposition of the four perovskites screened.

3. EXPERIMENTAL TECHNIQUES

3.1 Surface area measurement

For heterogeneous catalysis, it is desirable to express the rate constants in a form normalized to unit catalyst surface area. It is therefore important to be able to determine the true active surface area of the catalyst. Four different methods of measuring the active surface area were examined.

One of the most frequently used techniques for
determining catalyst surface area is low temperature
nitrogen (N_2) gas adsorption (BET) [33]. BET measurements
utilize the low temperature adsorption of a monolayer of
N_2 gas onto the surface of the sample. The N_2 gas is
desorbed, and the sample surface area is calculated from the
volume of gas desorbed and the cross-sectional area of a
N_2 molecule. BET can be used to measure catalyst surface
areas of both powders and Teflon-bonded electrodes.

Double layer capacitance has been used to measure
surface areas of electrodes of many metals [34,35] and some
metal oxides [36]. In theory, the double layer capacitance
of a catalyst should be directly proportional to surface
area. The total capacitance can be measured by cyclic
voltammetry using the equation,

$$C = i/(dV/dt) \quad (5)$$

where C is the double layer capacitance in farads, i is the
current in milliamps, and dV/dt is the scan rate in
millivolts per second (mV/s). It is assumed that the total
capacitance is equal to the double layer capacitance. If
the capacitance per unit surface area of the catalyst is
known, electrode capacitance can be used to calculate the
electrochemically active catalyst surface area.

Hydrogen adsorption has been used to measure the
electrochemically active catalyst surface areas of Pt
electrodes [36-38]. Surface area determination is based
upon the measurement of the coulombic charge associated with

9

the removal of an adsorbed monolayer of hydrogen, which is electrochemically oxidized according to the equation,

$$H_{ads} = H^+ + e^- \quad (6).$$
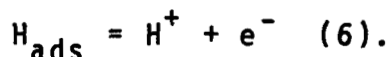
The Pt surface area is calculated using the conversion of 210 microcoulombs per cm^2 [37].

It is also possible to calculate catalytic surface areas from powder surface area and catalyst loading. These calculations are based on the assumption that 100% of the catalyst surface area is available.

3.2 Studies which use catalyst powder

Three of the methods used to determine HO_2^- decomposition rate constants require catalyst powder. Two of these methods monitor the rate of production of O_2 gas which is formed as a reaction product. The third method monitors the HO_2^- concentration directly by measuring the diffusion limiting current at a rotating disk electrode (RDE). The experimental conditions encountered in the three studies are very similar.

3.2A Gasometric studies

In the first method, the oxygen volume is monitored versus time using the gasometric assembly given in Figure 2 [29,30]. Fifty milligrams (mg) of the catalyst is dispersed in 50 milliliters (ml) of 31% KOH within the sealed flask.
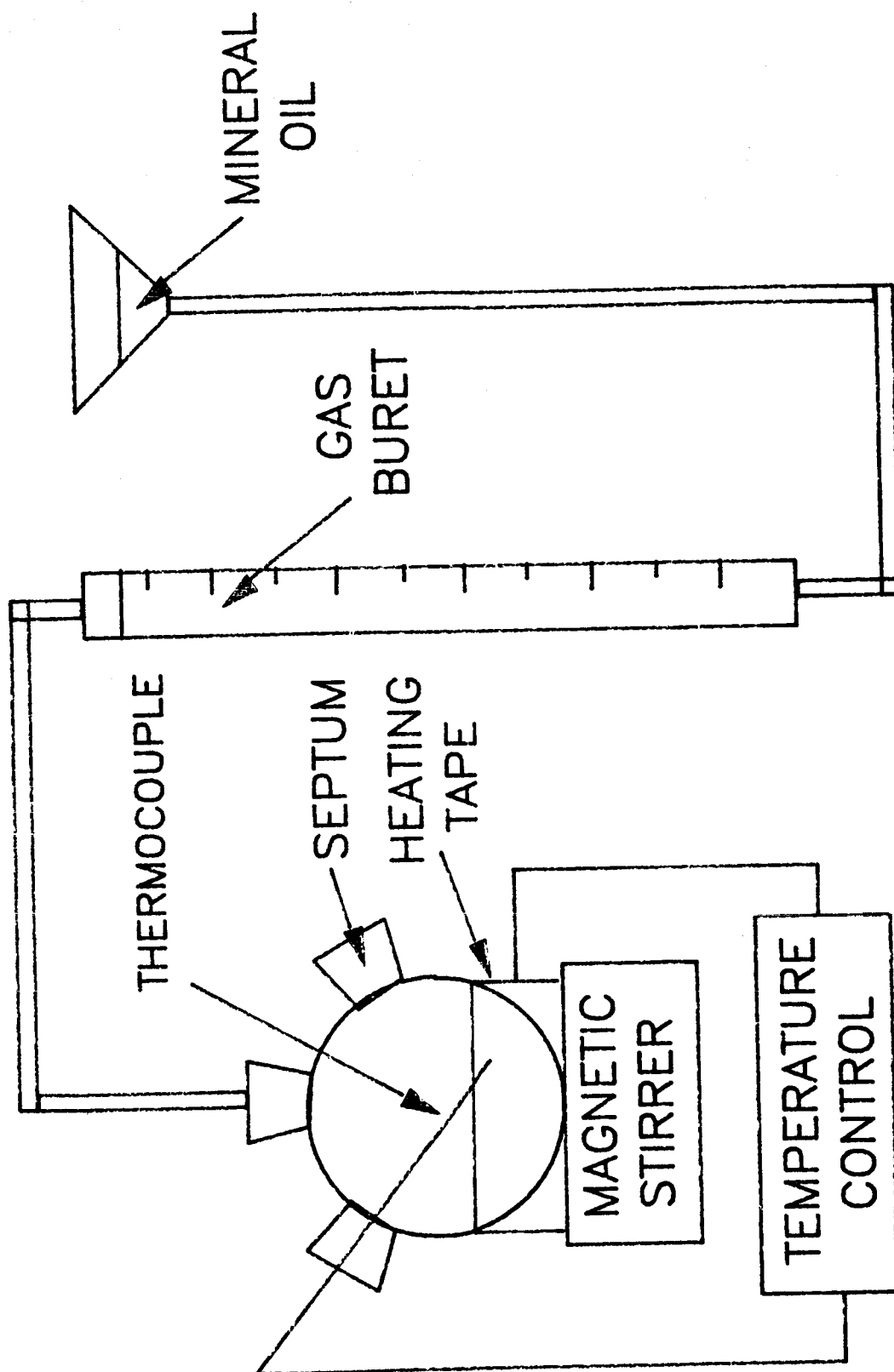
Figure 2: Experimental apparatus for gasometric studies.

Five ml of 5% H_2O_2 is injected into the system through the septum, and the rate of oxygen evolution is measured at 25 ^OC and atmospheric pressure, as the oxygen gas displaces mineral oil in the gas buret. The first order pseudo-homogeneous rate constant (k') for reaction (4) can be determined from this data using the equation,

$$ln(V_m - V_t) = ln(V_m) - k'xt \quad (7)$$

where V_m is the maximum oxygen volume (ml), and V_t is the oxygen volume (ml) at time t [30]. A plot of $ln(V_m - V_t)$ versus time in seconds (sec) should yield a straight line with a slope equal to k'. The first order heterogeneous rate constant (k_h) is conveniently expressed in a form normalized to catalyst surface area, and can be calculated from k' using the relationship,

$$k_h = k'xV_l/M_cxA_c \quad (8)$$

where V_l is the solution volume (ml), M_c is the catalyst mass in grams (g), and A_c is the catalyst surface area in cubic centimeters (cm^3) [31].

3.2B Oxygen probe studies

In the second method, the gas phase oxygen concentration is measured directly using an oxygen meter. The experimental apparatus used in oxygen probe studies is given in Figure 3. In an oxygen probe, the oxygen gas diffuses through a Teflon membrane and is electrochemically
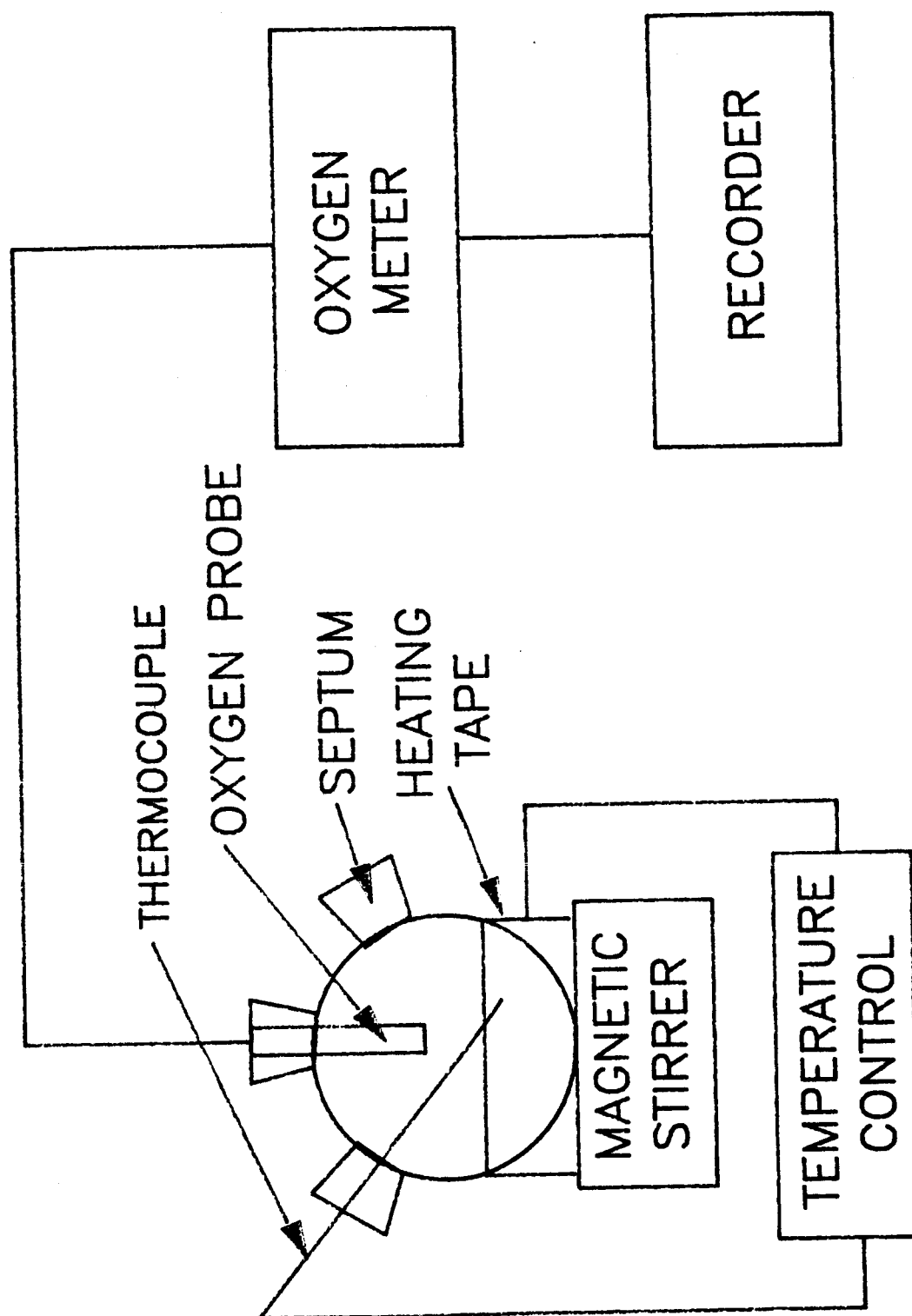
Figure 3: Experimental apparatus for O_2 probe studies.

reduced inside the probe. The resulting current is directly related to the gas phase oxygen concentration. Fifty mg of the catalyst is dispersed in 50 ml of 31% KOH within the reaction flask. The flask is purged with N_2, and 5 ml of 5% H_2O_2 is injected into the system. The gas phase oxygen concentration is monitored versus time using a recorder. These data can be used to calculate the pseudo-homogeneous rate constant (k') using the equation,

$$ln(\%O_{2m} - \%O_{2t}) = ln(\%O_{2m}) - k'xt \quad (9)$$

where $\%O_{2m}$ is the maximum percent oxygen, and $\%O_{2t}$ is the percent oxygen at time t. A plot of $ln(\%O_{2m} - \%O_{2t})$ versus time (sec) should be linear with a slope equal to -k'. The first order heterogeneous rate constant (k_h) can be calculated from k' using equation (8).

3.2C Rotating disk electrode studies

The third method utilizes the rotating disk electrode (RDE) apparatus shown in Figure 4 [31]. Fifty mg of the catalyst is dispersed in 50 ml of 31% KOH within the electrochemical cell, and 5 ml of 5% H_2O_2 is added to the solution. The HO_2^- concentration is monitored versus time by measuring the diffusion limiting current for HO_2^- oxidation at the rotating disk. The HO_2^- concentration is calculated from the diffusion limiting current, I_L in amperes (A), using a rearranged form of the

14

PLATINUM COUNTER ELECTRODE

GOLD ROTATING DISK ELECTRODE

GLASS TUBING

31% KOH ELECTROLYTE

Hg/HgO REFERENCE ELECTRODE

GAS DISPERSION TUBE

N_2
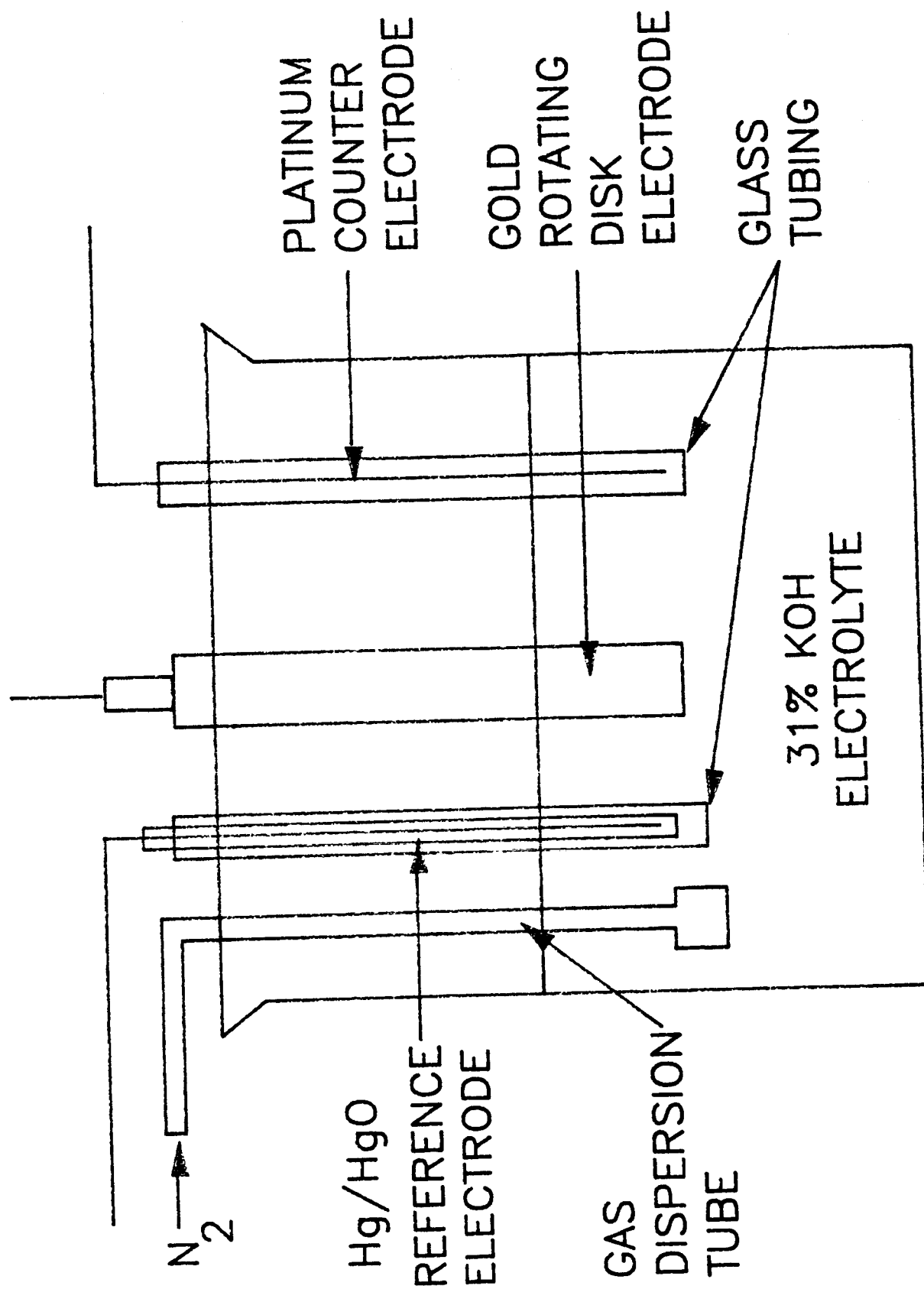
Figure 4: Electrolysis cell used in RDE studies

Levich equation [21],

$$C = I_L/(0.620 \times nFA_c \times v^{-1/6} \times D^{2/3} \times f^{1/2}) \quad (10)$$

where $n=2$, A_c is the electrode area (cm^2), v is the kinematic viscosity (cm^2/s), D is the diffusion coefficient (cm^2/s), and f is the rotation frequency in revolutions per minute (rpm). A first order plot of $\ln(C/Co)$ versus time (sec) should yield a straight line with a slope equal to $-k'$. As in the case of the gasometric and oxygen probe studies, equation (8) is used to calculate k_h from k'.

3.3 Studies which use Teflon-bonded electrodes

The last two methods for determining HO_2^- decomposition rate constants utilize Teflon-bonded electrodes which are fabricated from the catalysts [40]. The Teflon allows for diffusion of oxygen gas into the electrode pores and acts as a binder for the catalyst powder. Carbon is often added during the fabrication process to increase conductivity, prevent catalyst agglomeration, and to insure reversibility of reaction (2) [40]. The mixture is pressed onto a nickel screen which acts as a current collector and adds to the structural integrity of the electrode.

3.3A Open circuit potential decay studies

HO_2^- decomposition is monitored by open circuit potential decay [31] using the floating electrode half-cell apparatus [41,42] given in Figure 5. The experiments are conducted in 31% KOH at 25 $^\circ$C and one atmosphere of oxygen. In this experiment a constant cathodic current between .1 and 2 mA is applied to the working electrode until a steady-state is reached. Afterwards, the current is interrupted and the potential decay of the working electrode is monitored versus time. A plot of potential decay in volts (V) versus time (sec) can be used to calculate the first order heterogeneous decomposition rate constant (k_h), using the Nernst equation [40], and the relationship [31] (see Appendix),

$$(V_1/A_c) \times \ln(C/C_0) - (RTC_t/4F^2A_c) \times (1/C - 1/C_0) = -k_h \times t \quad (11)$$

where C is the concentration in moles per cubic centimeter (mol/cm^3) at time t, C_0 is the initial concentration (mol/cm^3), V_1 is the liquid volume within the electrode pores (cm^3), A_c is the catalyst surface area (cm^2), and C_t is the total capacitance in farads (F). This equation considers both the first order catalytic decomposition of HO_2^-, and the further production of HO_2^- by the discharge of the total capacitance after the current has been interrupted. At short times or large

17

Pt working electrode lead wire

Thermocouple-controller

Teflon bracket

Pt contact to Working electrode

Pt counter electrode lead wire

Electrolyte level

Hg/HgO reference lead wire

Gas from presaturator

Hg/HgO reference electrode
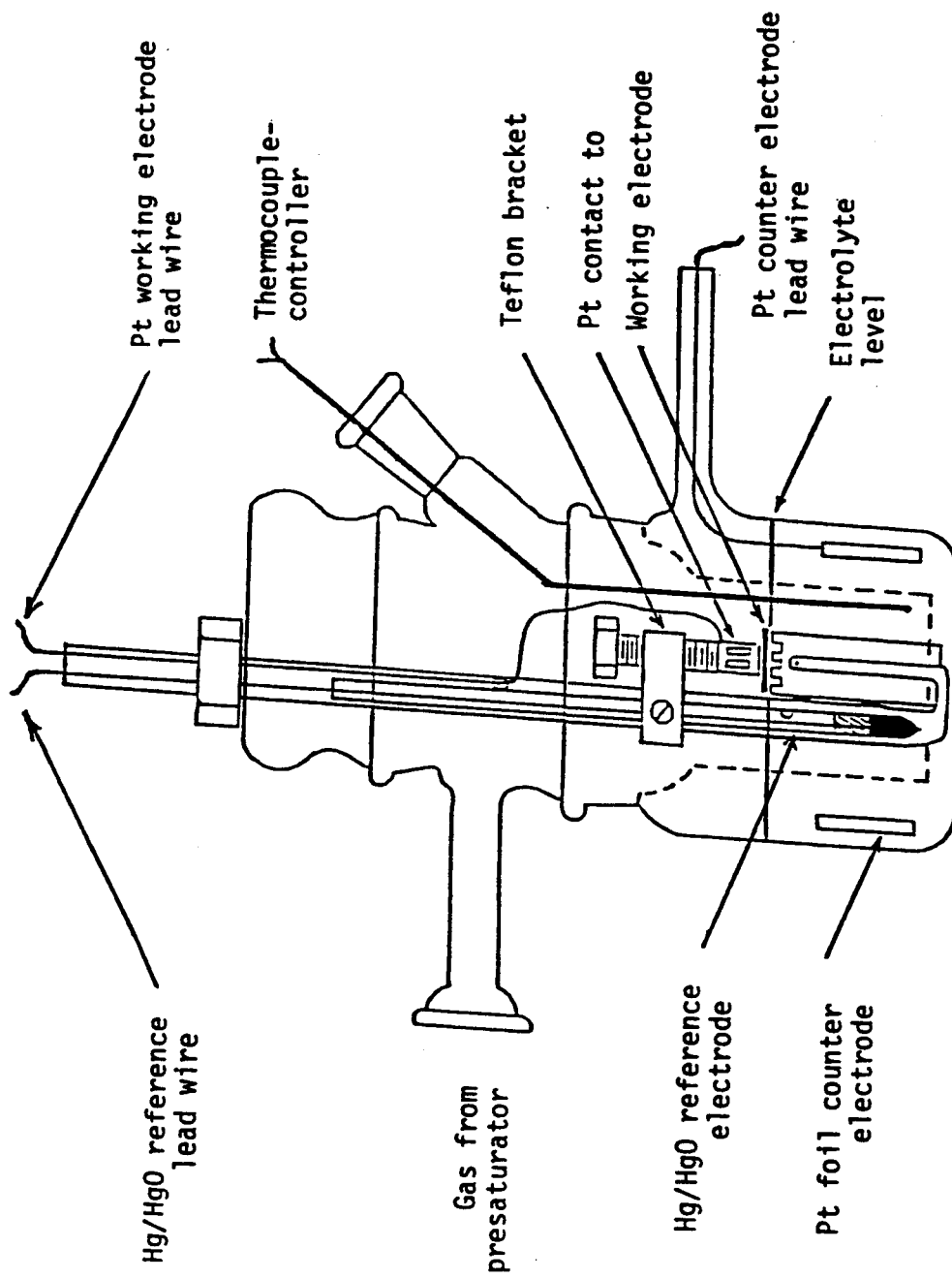
Pt foil counter electrode

Figure 5: Diagram of the Giner-type floating half-cell.

18

HO_2^- concentrations the first term on the left hand side of the equation dominates, and a first order dependence is observed. A plot of $\ln(C/C_0)$ versus time will yield a straight line with a slope equal to $-(A_c/V_1)xk_h$. At long times or small HO_2^- concentrations the second term on the left hand side of equation (11) dominates and a pseudo-second order dependence is observed. A plot of $(1/C - 1/C_0)$ versus time (sec) should be linear with a slope equal to $(4F^2A_c/RTC_t)xk_h$.

3.3B Steady-state polarization studies

HO_2^- decomposition rate constants can also be determined by steady-state polarization (SSP) measurements, using the floating half-cell apparatus described previously. In this technique, a polarization curve is obtained galvanostatically by applying a cathodic current between 10 and 100 mA and measuring the corresponding steady-state voltages. This data can be used to generate Tafel plots using the Tafel equation [21],

$$N = (2.3RT/anF)x\log(i_0) - (2.3RT/anF)x\log(i) \quad (12)$$

where N is the overvoltage vs RHE (V), R is the gas constant, T is the temperature in Kelvin, a is the transfer coefficient, n is the number of moles of electrons transferred, F is the Faraday constant, i_0 is the exchange current (A) per cm^2 of geometrical surface area, and i is the polarizing current (A/cm^2). A plot of the

19

polarization versus the log of the current should yield a straight line with a Tafel slope equal to -2.3RT/anF. If oxygen reduction to HO_2^- is fast, and the decomposition of HO_2^- is the rate limiting step, then the Tafel slope (assuming a=0.5) is -29.6 mV/decade at 25 ^{O}C. For an electrode whose Tafel slope approaches this value, a decomposition rate constant can be calculated from the Tafel-linear region of the polarization curve, using the Nernst equation [40] and the relationship [31],

$$I = 2FA_c \times k_h \times C_{HO2^-} \quad (13)$$

where I is the polarizing current in amperes (A), F is the Faraday constant, A_c is the catalyst surface area (cm^2), C_{HO2^-} is the surface perhydroxyl ion concentration (mol/cm^3), and k_h is the first order heterogeneous decomposition rate constant (cm/s). A plot of current (A) versus the concentration of peroxide (mol/cm^3) should yield a straight line with a slope equal to $2FA \times k_h$.

II. EXPERIMENTAL

1. REAGENTS

The potassium permanganate ($KMnO_4$) solution was prepared by dissolving 3.21 gs $KMnO_4$ (C.P. Baker Co. lot #12549) in one liter of nanopure water. The solution was boiled gently for 20 minutes, cooled, and filtered through a sintered glass disk. The filtrate was collected in a bottle which was cleaned with chromic acid and distilled water. The solution was standardized using .300 gs of sodium oxalate (Baker Chemical Co. Primary Standard, lot #43251) which was dried in an oven at 110 ^{o}C for two hours. The sodium oxalate was dissolved in 240 ml of concentrated sulfuric acid. 35 ml of the $KMnO_4$ solution was added over a three minute period and the solution was heated to 55 ^{o}C. The solution was then titrated until a faint pink color persisted for 30 seconds [43].

The 5% peroxide solution was prepared by pipetting 10 ml of 90% unstablized peroxide (FMC Corporation, Specialty Chemicals Division) into a 250 ml volumetric flask and diluting to the mark with nanopure water. This solution was titrated with the $KMnO_4$ prepared previously. Ten ml of the peroxide solution was pipetted into a 300 ml beaker which contained 100 ml of distilled water and 10 ml of concentrated sulfuric acid. The solution was titrated until

21

a faint pink color persisted for 30 seconds [43].

The 31% KOH solution was prepared using a 45% weight per cent (w/w) KOH solution (Fisher Scientific Company, Lot #711940). The specific gravity of the KOH was measured by placing 25 ml of the solution in a volumetric flask and weighing the contents. The weight per cent of the solution was obtained from a table of concentration versus specific gravity [44].

2. OXYGEN PROBE STUDIES

2.1 General

The experimental apparatus used for oxygen probe studies is given in Figure 3. The assembly consisted of a Beckman Model 0260 Oxygen Analyzer with a Fieldlab #39553 Oxygen Sensor, a Cole-Parmer Digisense Temperature Controller, and a Fisher Recordall Series 2000 recorder. A small opening in the septum insured that the pressure inside and outside the flask was in equilibrium. The oxygen meter was calibrated at 0.0% by placing the probe in a vacuum flask which was purged with N_2 gas. For aqueous measurements, the probe was placed in distilled water which had been air saturated by shaking vigorously and allowing to stand for two minutes. A table of oxygen concentration at various temperatures gives the standard oxygen

concentration. For gas phase measurements the probe was calibrated at 20.9% oxygen by exposing the probe to the air. All measurements were made in 31% KOH at 25 $^{\circ}$C and atmospheric pressure.

2.2 Measurement of Henry's Law gas constant

The Henry's Law gas constant was measured at 25 $^{\circ}$C for the 31% KOH solution in the following way. The solution was saturated with air by vigorously shaking it and allowing it to stand for two minutes. At one atmosphere total pressure the partial pressure of oxygen is .209 atmospheres (atm). The oxygen meter was used to measure the dissolved oxygen, and the Henry's Law gas constant (k_H) was calculated using the equation,

$$k_H = C/P_{O2} \quad (12)$$

where C is the liquid phase oxygen concentration in moles per liter (M), and P_{O2} is the oxygen partial pressure in atmospheres.

2.3 Determination of oxygen leakage rate

It was necessary to measure the rate of leakage of oxygen gas into the system through the hole in the septum. To accomplish this 50 ml. of the KOH solution was placed in the flask, and the flask was purged with N_2. When the meter read 0% oxygen the N_2 gas was turned off and the per

cent oxygen was monitored versus time using a strip chart
recorder.

2.4 Determination of the autodecomposition rate constant

The autodecomposition rate constant for the unstablized
peroxide was measured in the following way. Fifty ml of the
KOH solution was placed in the flask and the flask was
purged with N_2. When the meter read 0%, 10 ml. of the 5%
unstablized hydrogen peroxide was injected into the system.
The per cent oxygen was monitored with a strip chart
recorder and the autodecomposition rate was calculated using
these data.

2.5 Determination of catalytic decomposition rate constants

For gas phase oxygen measurements 50 milligrams (mg) of
the catalyst was placed in a three-neck 250 ml. round-bottom
flask, and 50 ml. of the KOH solution was added. The system
was immersed in a thermostated water bath, the solution was
stirred, and the flask was purged with N_2 gas. When the
meter read 0% oxygen, the N_2 was turned off and a known
amount of the 5% peroxide (from one to ten ml) was injected
through the septum into the flask. A strip chart recorder
was used to monitor the per cent oxygen in the gas phase

versus time. The first order heterogeneous rate constant
was calculated from these data using equations (8) and (9).

3. GASOMETRIC STUDIES

3.1 General

Gasometric studies were conducted using the apparatus
given in Figure 2. The assembly consisted of a 50 ml. gas
buret which was connected to a 250 ml. 3-neck round bottom
flask with Tygon tubing, a water bath, and a Cole-Parmer
Digisense Temperature Controller. In this experiment the
decomposition of hydrogen peroxide generates oxygen gas
which displaces the mineral oil in the gas buret. All
experiments were conducted at 25 ^{o}C and atmospheric
pressure.

3.2 Measurement of gas leakage rate

It was necessary to determine the leakage rate of the
system in order to obtain the true oxygen volume. This was
accomplished by charging the sealed system with air from the
syringe until the gas volume in the buret read 50 ml. and
monitoring the decrease over a 30 minute time interval.

3.3 Determination of catalytic decomposition rate constants

In the gasometric studies 50 mg of the catalyst was placed in a 250 ml, 3-neck, round-bottom flask which contained 50 ml of the KOH solution. The system was sealed, and a known amount of the 5% hydrogen peroxide was injected through the septum into the flask. The volume of the oxygen gas in the buret was read and recorded at 30 second time intervals until a maximum was reached. The first order heterogeneous rate constant was calculated from these data using equations (7) and (8).

4. ROTATING DISK ELECTRODE (RDE) STUDIES

4.1 General

RDE studies [31,45,46] were conducted using the experimental apparatus given in Figure 4. The working electrode was a gold disk with a surface area of 0.196 cm^2 (Pine Instrument Co.). The counter electrode was a 25 cm length of 20 gauge platinum wire. The mercury/mercuric oxide (Hg/HgO) reference electrode [36] was fabricated from a 15 cm length of soft glass (3 mm O.D.). A small hole (.4mm) was sandblasted in the tube approximately 2 cm from one end, and the end of the tube nearest the hole was

sealed. A drop of mercury (Bethlehem Apparatus Co. Inc., Hellertown, Pa.) was mixed with 0.5 gs of mercuric oxide (Mallindcrodt) in a mortar and pestle, and a long syringe was used to place the mercury and the mercuric oxide mix in the tube. A 20 cm platinum wire was inserted into the tube, and the electrode was allowed to stablize in 31% KOH for two days before use.

Current-potential curves were obtained using the electrochemical cell, a AFMSR rotator (Pine Instrument Co.), a Model AFRDE4 Potentiostat (Pine Instrument Co.), and a Model 530 X-Y recorder (Esterline Co.). The disk electrode was pretreated before each measurement by stepping the potential to +.250 V vs Hg/HgO for 10 seconds and then to -.300 V vs Hg/HgO for 10 seconds to remove any oxides formed during the anodic step. All measurements were made in 31% KOH at 25 $^{\circ}$C.

4.2 Determination of autodecomposition rate constant

The autodecomposition rate constant for HO_2^- was measured by placing 50 ml of 31% KOH in the electrochemical cell and adding 5 ml of the 5% HO_2^-. The RDE was rotated at 3000 revolutions per minute (rpm) and the limiting current was measured by sweeping the potential at 20 mV/s between -.070 V and +.250 V vs Hg/HgO at five minute time intervals. The HO_2^- concentration was calculated from this data using equation (10). The autodecomposition

27

rate constant was calculated from the slope of a plot of $\ln(C/C_0)$ versus time (sec).

4.3 Catalytic decomposition rate constants

The catalytic decomposition rate constants for the catalyst powders were determined in the following way. 50 ml of the 31% KOH solution was added to the electrochemical cell along with 50 mg of the catalyst and the RDE was rotated at 3000 rpm. The limiting current was measured by sweeping the potential at 20 mV/s between -.070 V and +.250 V versus Hg/HgO at time intervals between one and five minutes, depending on the rate of decomposition. The HO_2^- concentration was calculated from this data using equation (10). The pseudo-homogeneous first order rate constant (k') was calculated from the slope of a plot of $\ln(C/Co)$ versus time in seconds. The first order heterogeneous rate constant (k_h) was calculated from k' using equation (8).

5. OPEN CIRCUIT POTENTIAL DECAY STUDIES

5.1 General

Open circuit potential decay measurements were carried out on Teflon-bonded electrodes which were fabricated using

high surface area electrocatalyst, a Teflon support, and, in many cases, carbon. The sources and compositions of the electrodes used in this study are summarized in Table 1. Catalyst syntheses and electrode fabrication techniques are given elsewhere [40,47-50]. The electrodes were cut into one cm^2 disks which were used in the floating electrode half- cell apparatus given in Figure 5. The half-cell consisted of a working electrode previously described suspended on the surface of a 31% KOH solution, a Hg/HgO reference electrode [36], and a platinum foil counter electrode. Both the half- cell and a presaturator were wrapped in heating jackets to maintain a constant temperature of 25 ^{o}C. Oxygen gas flowed through the presaturator which contained 31% KOH, and into the half cell where it was electrocatalytically reduced within the pores of the working electrode. In addition to the presaturator and the half cell, electrochemical measurements were carried out using a Model 273 Galvanostat/Potentiostat (Princeton Applied Research Corp.), and an Esterline Angus Model 530 X-Y recorder (Esterline Corp.). Electrodes were pretreated by scanning to 200 milliamps (mA) at 1.0 mA per second (mA/s).

5.2 Open circuit potential decay measurements

In open circuit potential decay measurements [31,40] a cathodic current was applied to the working electrode and

29

Table 1: Electrode sources and loadings.

Electrode #	Loading (per cm^2)	Source
1	5 mg Pt on 5 mg Vulcan XC-72	Electro-media Inc. (New Jersey)
2	7 mg Pt, "unsupported" Used as an anode in H_2-O_2 alkaline fuel cells.	Hughes Aircraft Co. (El Segundo CA)
3	.5 mg Au on acetylene black Average particle size of about 45 angstroms. [a]	Electro-Chem Inc. (Woburn, MA)
4	20 mg of "unsupported" Au with 10% added Pt. Particle sizes range from about 100 angstroms to several hundred angstroms. Some alloying. [a]	International Fuel Cells Corp. (South Windsor,CT)
5	CoTMPP catalyzed carbon black, Proprietary catalyst	Electro-media Inc. (New Jersey)
6	$La_{.5}Pb_{.5}MnO_3$, 1.3 mg on acetylene black	ELTECH Systems Corp. (Fairport Harbor,OH)

[a] Singer J., and Srinivasan, V., Evaluation Parameters for the Alkaline Fuel Cell Oxygen Electrode, NASA Technical Memorandum 87155.

the voltage was allowed to reach a steady-state value.
Afterwards, the current was interrupted and the voltage
decay of the working electrode was monitored versus time
using a recorder. Applied currents ranged from .1 mA to
about 2.0 mA. These data were used to determine catalytic
decomposition rate constants using equation (11).

5.3 Determination of total capacitances

The total capacitances of the electrodes were measured
using cyclic voltammetry (CV). The presaturator and
half-cell were purged with N_2 gas for 4 hours. The
electrode potential was scanned between -0.400 volts (V) and
+0.300 V vs. Hg/HgO, and the non-Faradaic region was
obtained from the voltammogram. This region usually lies
between +0.05 V and +0.20 V versus Hg/HgO. A voltammogram
was obtained by scanning this region at a scan rate of 10 mV
per second or less. This data can be used to obtain the
total capacitance in farads (F) using equation (5).

5.4 Determination of Electrode Pore Volumes

The pore volume was determined by measuring the weight
loss of the used electrode after careful washing with hot
distilled water and drying in an oven at 150 $^{\circ}$C for two

hours. The loss of weight was assumed to be due to loss of KOH solution from the electrode pores. The pore volume was calculated using the conversion of 1.3 g KOH per cm^3 KOH at 25 ^{o}C.

6. STEADY-STATE POLARIZATION STUDIES

6.1 General

Steady-state polarization (SSP) studies were carried out using the same apparatus described in the general section of the OCPD studies (see section 5.1). Experiments were conducted in 31% KOH at 25 ^{o}C.

6.2 Polarization measurements

Polarization curves were obtained galvanostatically by applying a cathodic current between 10 and 100 mA, and measuring the steady-state voltage. All curves were corrected for ohmic polarization using an ESC model 800 IR measurement device (Electrosynthesis Co.). A Tafel plot was generated from this data using equation (12). The heterogeneous decomposition rate constant (k_h) was calculated from the polarization data using equation (13).

7. MEASUREMENT OF CATALYST SURFACE AREA

7.1 Brunauer-Emmet-Teller (BET) surface area measurements

BET surface area measurements [33] were carried out on
the catalyst powders and the Teflon-bonded electrodes using
a Model 4200 Automatic Surface Area Analyzer (Leeds and
Northrup Instruments). The instrument was calibrated at
zero square meters (m^2) in the absence of a sample and at
15.23 m^2 by injecting 5 ml of air into the septum. A
sample weighing between .01 g and .10 g was placed in the
sample holder and inserted into the preparation station.
The sample was heated at 150 $^{\circ}$C for 1 hour to remove
moisture. The sample was then placed in the test station
and immersed in liquid N_2. The instrument will
automatically give a reading of the total surface area in
m^2.

7.2 Measurement of Pt surface area by hydrogen adsorption

The surface area of the platinum electrodes were
measured using hydrogen adsorption. Hydrogen adsorption
measurements were carried out on the Teflon-bonded
electrodes which were immersed in N_2-purged 1N H_2SO_4.
The electrode potential was scanned from +.080 V to +1.20 V

versus the dynamic hydrogen electrode (DHE) [36]. The area under the hydrogen adsorption peak was integrated and the surface area was calculated using the conversion of 210 microcoulombs per cm^2 [37,38].

7.3 Surface area measurement by scanning electron microscopy

The average particle sizes of the gold catalyst particles present in electrodes 3 and 4 were determined by SEM [60]. The surface area (A_c) can be calculated, assuming spherical particles, using the equation,

$$A_c \ (m^2/g) = 30000/[\ rxD \ ] \ (14).$$

where r is the particle radius in angstroms, and D is the density of the catalyst in grams per cubic centimeter (g/cm^3).

7.4 Surface area measurement by total capacitance

If the capacitance per unit surface area of the catalyst is known, it is possible to calculate the surface area of the Teflon-bonded electrodes based on electrode capacitance [34,51]. The procedure for measuring electrode capacitance is given in section 5.3.

III. RESULTS

1. SURFACE AREA MEASUREMENTS

The sources, preparation, and results of the surface area measurements of the catalyst powders are summarized in Table 2. All powder surface areas were measured by BET. The CoTMPP and La$_{.5}$Pb$_{.5}$MnO$_3$ powders were used to fabricate electrodes numbered five and six respectively (see Table 1).

Table 2: Powder sources and surface area measurements.

Catalyst	Surface Area (m^2/g)	Preparation/Source
platinum	13.8 [a]	Particles by reduction of H_2PtCl_6 (J. Bishop & Co.) [34]
gold	4.84 [b]	Particles by reduction of $HAuCl_4$ (Physical Sciences) [49]
CoTMPP	173 [a]	CoTMPP catalyzed carbon black (EMC) [50]
La$_{.5}$Pb$_{.5}$MnO$_3$	14.5 [a]	Coprecipitation followed by thermal decomposition at 600 ^{o}C (Case Western Reserve University) [47]

[a] measured by the author
[b] measurement provided by Physical Sciences Inc.

It should be noted that the platinum and gold powders used in oxygen probe, gasometric, and RDE studies are not the same as the powders used in the fabrication of electrodes numbered one, two, three, and four.

The results of the surface area measurements of the Teflon-bonded electrodes, and the techniques used to determine the surface areas are given in Table 3. All electrode surface areas are given in units of m^2 of true surface area per cm^2 of geometrical surface area.

Hydrogen adsorption was used to determine the electrochemical surface area of a platinum disk of 0.196 cm^2 geometrical surface area. The disk was polished by hand with 5, 0.3, and 0.05 micron alumina. The cyclic voltammogram of the Pt disk electrode is given in Figure 6. The true surface area was determined to be 0.37 cm^2, yielding a roughness factor of about two. The total capacitance of the electrode as determined by cyclic voltammetry was found to be 48 microfarads. From these results, the capacitance per cm^2 for platinum was calculated to be about 128 microfarads. This value was used to calculate the surface area of the Hughes platinum electrode. The surface area of the Hughes platinum was also determined by BET, hydrogen adsorption, and calculations based on the powder surface area and catalyst loading.

Attempts were also made to measure the capacitance of the gold disk electrode. The capacitance of the electrode was found to be fifty microfarads. However, the true gold
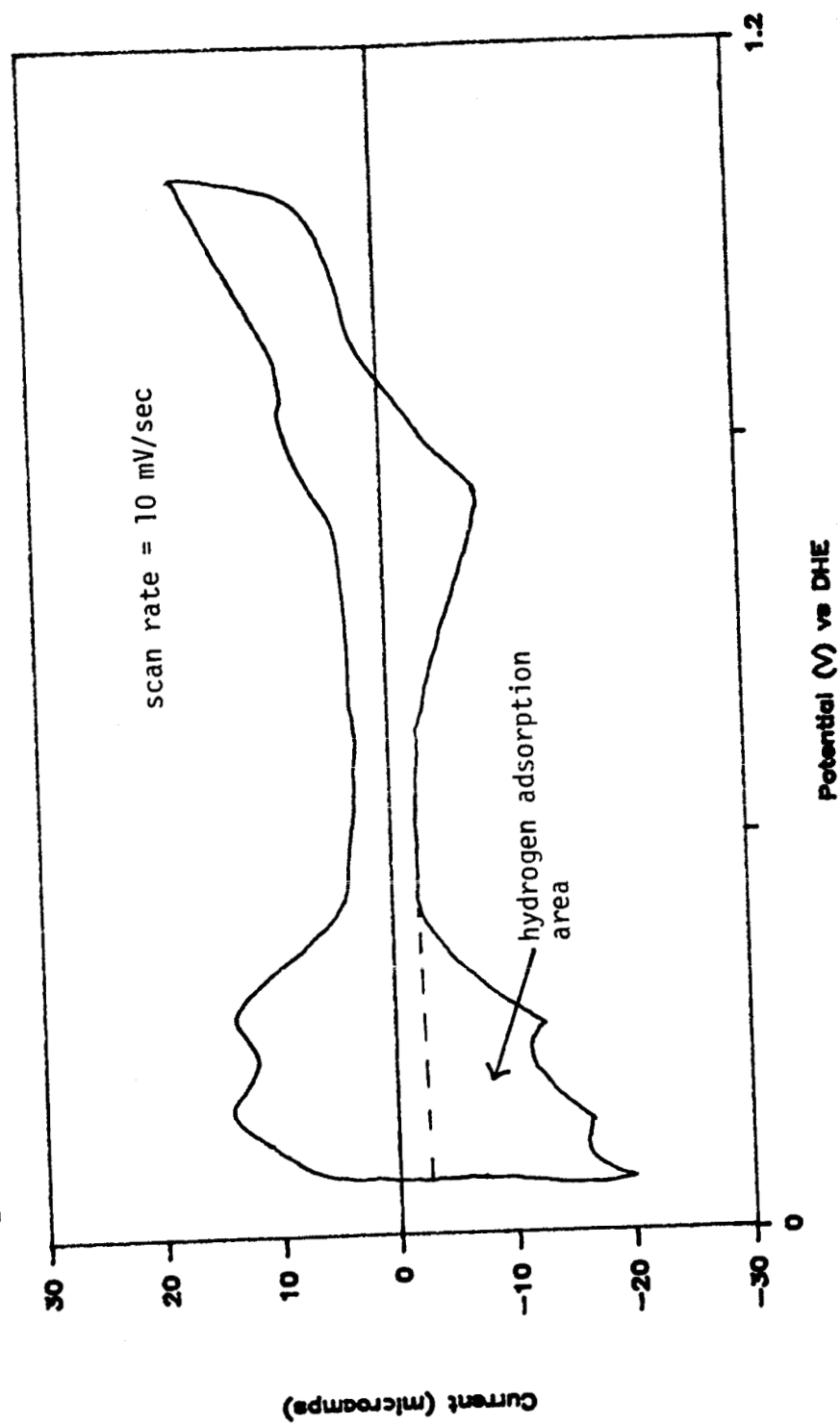
CYCLIC VOLTAMMOGRAM OF PT ELECTRODE

Figure 6: Cyclic voltammogram of a .196 cm^2 Pt disk in 1 N sulfuric acid.

Table 3: Surface area measurements of Teflon-bonded electrodes.

Electrode #	Description (per cm^2)	Surface Area (m^2/cm^2 geo)	Technique
1	5 mg Pt on XC72 (EMC)	4.6 .43 .20	BET H_2 adsorption calculated [b]
2	7 mg Pt "un-supported" (Hughes)	.11 .22 .10 .11	calculated [b] BET H_2 adsorption capacitance
3	.5 mg Au on acetylene black(Elec-trochem)	.035	calculated [a]
4	20 mg Au,10% Pt "unsup-ported"(IFC)	.16 .22 .22	capacitance BET calculated [a]
5	CoTMPP cata-lyzed carbon black (EMC)	1.9 .99	calculated [b] BET
6	$La_{.5}Pb_{.5}MnO_3$ 1.3 mg on acetylene black (ELTECH)	.02	calculated [b]

[a] calculated from electrode SEM [60] and electrode loading

[b] calculated from powder BET and electrode loading

surface area could not be determined, therefore, it was necessary to assume a roughness factor of two. This assumption was reasonable as the gold and platinum disks were polished in a similar fashion. Using a value of 0.40 cm^2 as the true surface area, the capacitance per cm^2 of gold is about 125 microfarads. This value was used to calculate the surface area of the IFC (formerly UTC) gold electrode. The surface area of the IFC gold electrode was also determined by BET, and calculations based on catalyst loading and electrode SEM measurements [60].

2. OXYGEN PROBE STUDIES

The Henry's Law gas constant was determined to be 3.5×10^{-4} M/atm for O_2 in the 31% KOH solution at 25 $^{\circ}$C. Since the oxygen solubility was low, presaturation of the 31% KOH solution was not required for the gasometric and oxygen probe experiments. Also, as a result of the low liquid-phase oxygen solubility, all oxygen probe measurements were carried out in the gas phase.

The autodecomposition rate as determined by oxygen probe measurements was several orders of magnitude smaller than the catalytic decomposition rates for gasometric, oxygen probe, and RDE experiments. For the oxygen probe studies, the rate of diffusion of oxygen into the system through the hole in the septum was about two orders of

magnitude smaller than the rate of oxygen production via HO_2^- decomposition. Results of HO_2^- decomposition measurements for the platinum powder using the oxygen probe apparatus are given in Figures 7A and 7B.

Oxygen probe experiments were conducted with platinum at different stirring rates to determine if mass transport was the rate limiting process. The results of these experiments are given in Figure 8. At stir rates above four, the initial rate of oxygen production was constant, therefore, if the solution is well stirred, mass transport should not be a problem.

The results of the oxygen probe studies using the four catalyst powders are summarized in Table 4. All rate

Table 4: First order rate constants (cm/s) for the four catalyst powders as determined by gasometric, oxygen probe, and RDE experiments in 31% KOH at 25 °C.

TECHNIQUE

		gasometric	oxygen probe	RDE
C A T A L Y S T	platinum (J. Bishop)	8.8×10^{-5}	9.1×10^{-5}	9.8×10^{-5}
	gold (PSI)	7.6×10^{-6}	8.0×10^{-6}	9.2×10^{-6}
	CoTMPP catalyzed carbon black (EMC)	1.3×10^{-6}	1.3×10^{-6}	2.2×10^{-6}
	La.$_5$Pb.$_5$MnO$_3$ (CWRU)	2.0×10^{-5}	1.9×10^{-5}	1.6×10^{-5}

OXYGEN PROBE DATA FOR PT

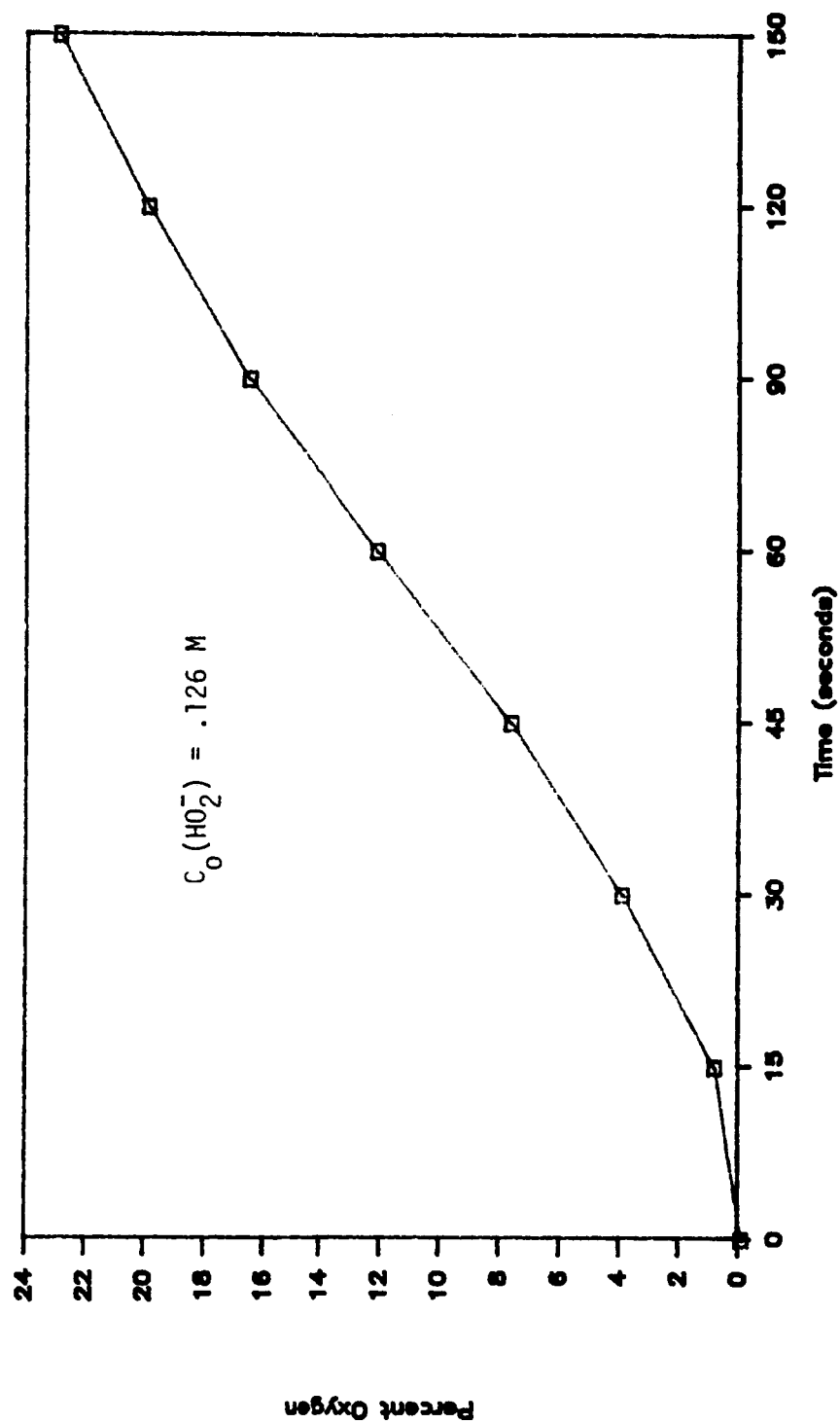$C_o(HO_2^-) = .126$ M

Time (seconds)

Percent Oxygen

Figure 7A: Oxygen probe data for 50 mg of Pt powder in 31% KOH at 25 ^oC.

OXYGEN PROBE PLOT FOR PT
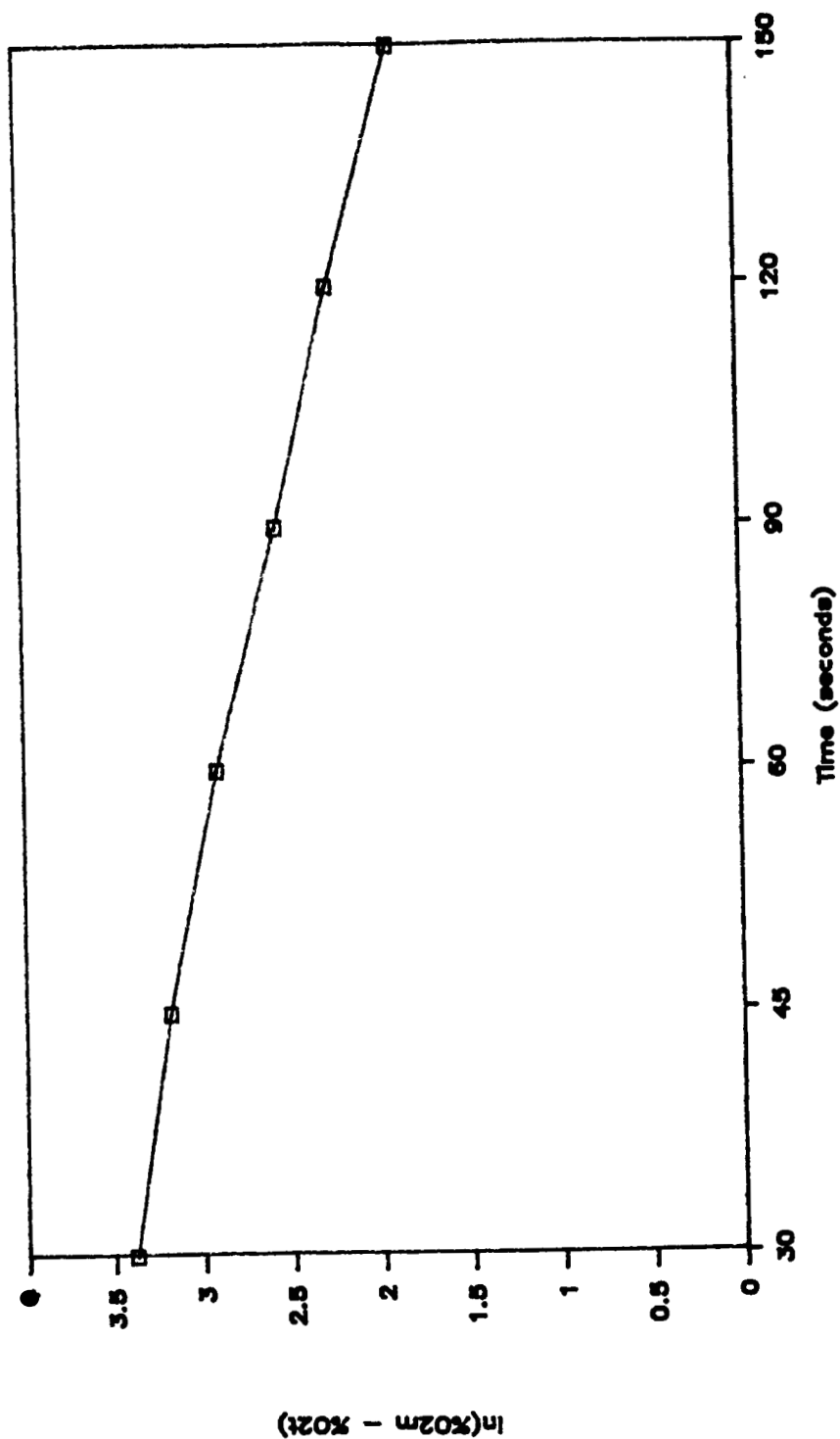
Figure 7B: Oxygen probe plot for 50 mg of Pt in 31% KOH at 25 °C.
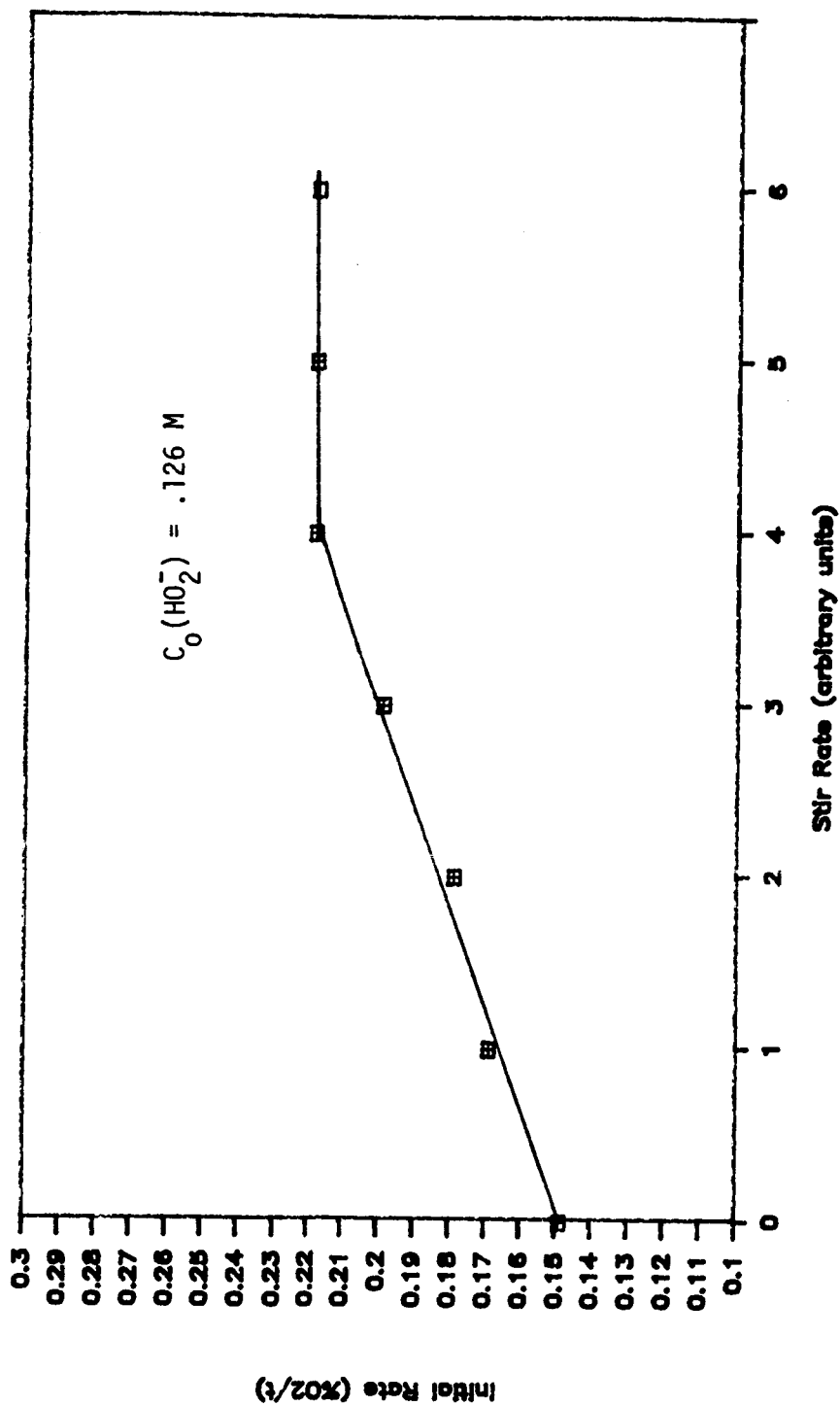
INITIAL RATE VERSUS STIRRING RATE

$C_0(HO_2^-) = .126$ M

Figure 8: Effect of stirring on the initial rate of production of O_2 for 50 mg of Pt powder in 31% KOH at 25 °C.

Initial Rate (%O2/t)

Stir Rate (arbitrary units)

constants have been normalized to unit catalyst surface area, and are given in units of centimeters per second (cm/s). All experiments were conducted in 31% KOH at 25 °C.

3. GASOMETRIC STUDIES

In the case of the gasometric studies, the leakage rate of oxygen gas out of the system was calculated to be about 0.50 ml/min and therefore oxygen volumes had to be corrected for the leak. Figures 9A and 9B are given as an example of the results obtained with the gasometric assembly.

The gasometric assembly was used to investigate the effect of catalyst wetting on the heterogeneous rate constant (k_h). Addition of one drop of Triton X-100 (a surfactant) to the catalyst suspension did not alter k_h for the platinum, gold, and La$._5$Pb$._5$MnO$_3$ catalysts. However, addition of a drop of Triton X-100 to the CoTMPP suspension increased k_h by a factor of three. This increase is assumed to be the result of increased wettability of the CoTMPP catalyst.

The results of the gasometric studies using the four catalyst powders are summarized in Table 4. All rate constants are normalized to unit catalyst surface area and are given in units of cm/s.
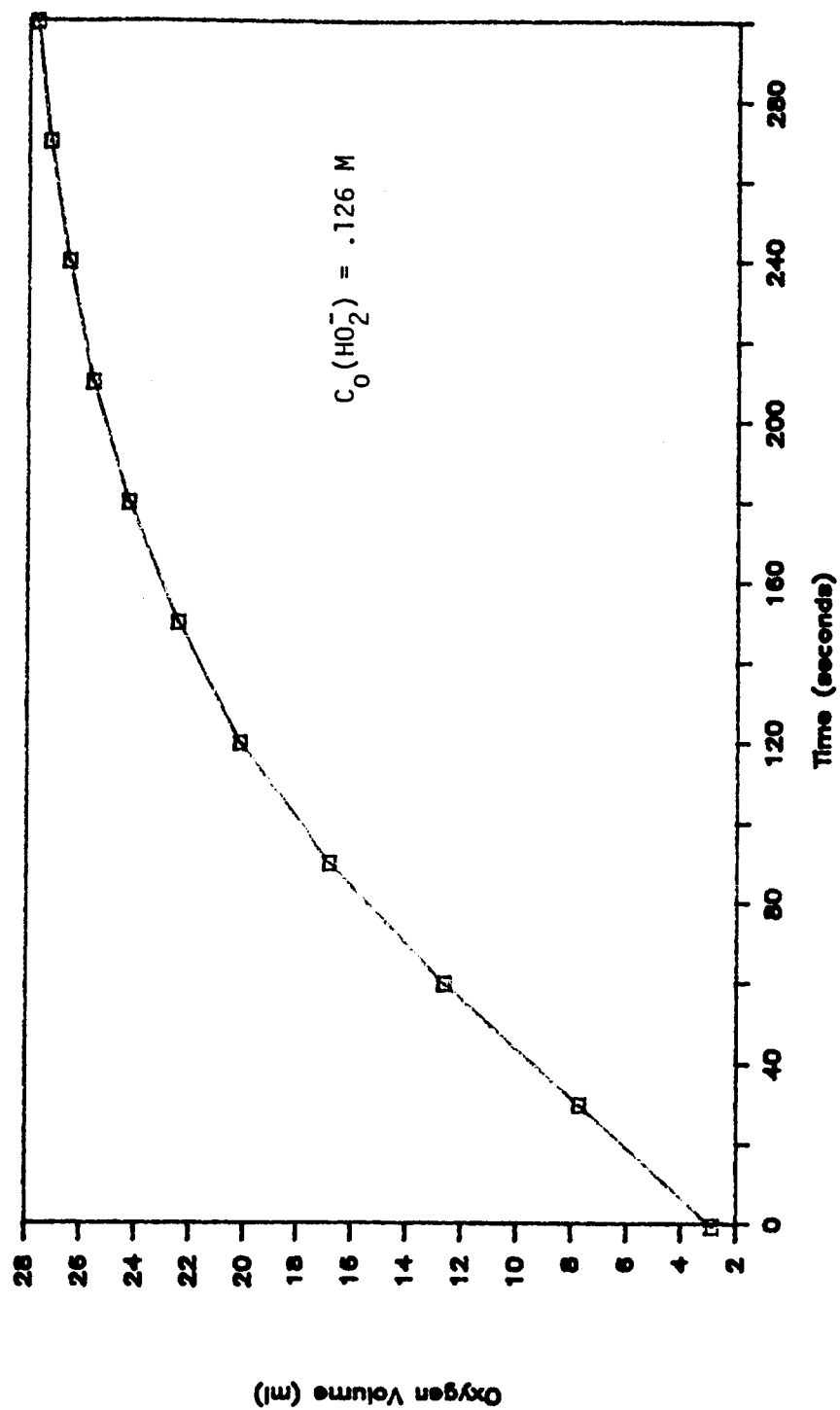
GASOMETRIC DATA FOR PT

$C_o(HO_2^-) = .126 \ M$

Time (seconds)

Oxygen Volume (ml)

Figure 9A: Gasometric data for 50 mg of Pt powder in 31% KOH at 25 ^oC.
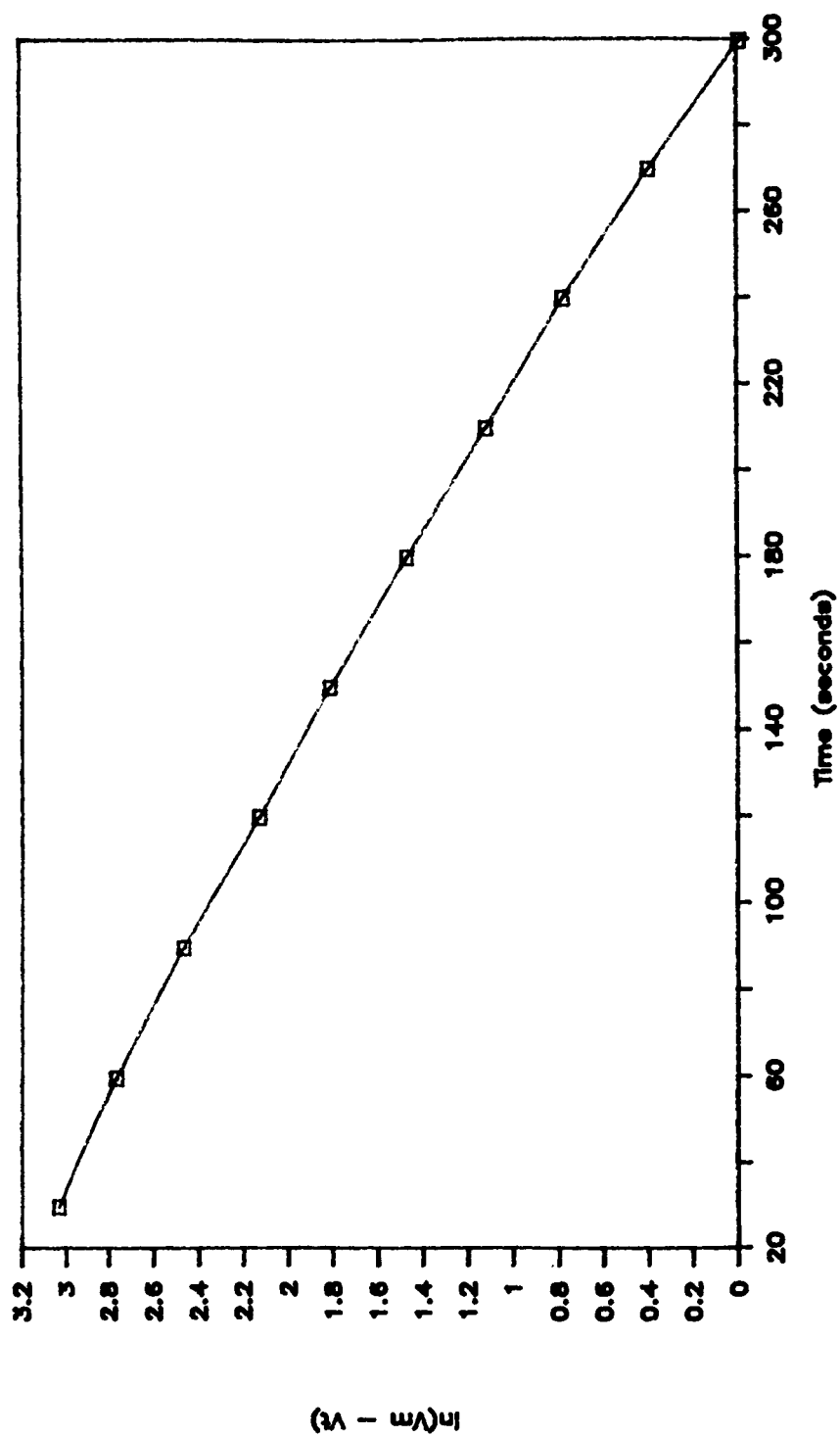
GASOMETRIC PLOT FOR PT

Figure 9B: Gasometric plot for 50 mg of Pt in 31% KOH at 25 °C.

46

4. ROTATING DISK ELECTRODE STUDIES

For the RDE studies, the surface areas of the catalyst powders were about three orders of magnitude larger than the surface areas of the gold disk and platinum counter electrodes. Therefore, the rate of HO_2^- decomposition due to the platinum counter electrode and the gold working electrode was negligible in comparison to the decomposition rate due to the added catalyst powder. The term $0.620nFAv^{-1/6}D^{2/3}$ was calculated from the slope of a plot of the limiting current versus $C_{H2O2}xw^{1/2}$ at rotation speeds between 1000 and 5000 rpm. This plot is shown in Figure 10. The value of the constant was determined to be $(1.61)x10^{-3}$ A/M(rpm)$^{1/2}$ for 31% KOH at 25 $^{\circ}$C. Results of decomposition studies for the platinum powder using the RDE apparatus are given in Figures 11A and 11B.

The results of the RDE studies using the four catalyst powders are summarized in Table 4. The rate constants are given in units of cm/s. All experiments were conducted in 31% KOH at 25 $^{\circ}$C.

PLOT OF CURRENT VERSUS ROTATION SPEED

Current (A)

0.0048
0.0046
0.0044
0.0042
0.004
0.0038
0.0036
0.0034
0.0032
0.003
0.0028
0.0026
0.0024
0.0022

1.32   1.86   2.28   2.63   2.94
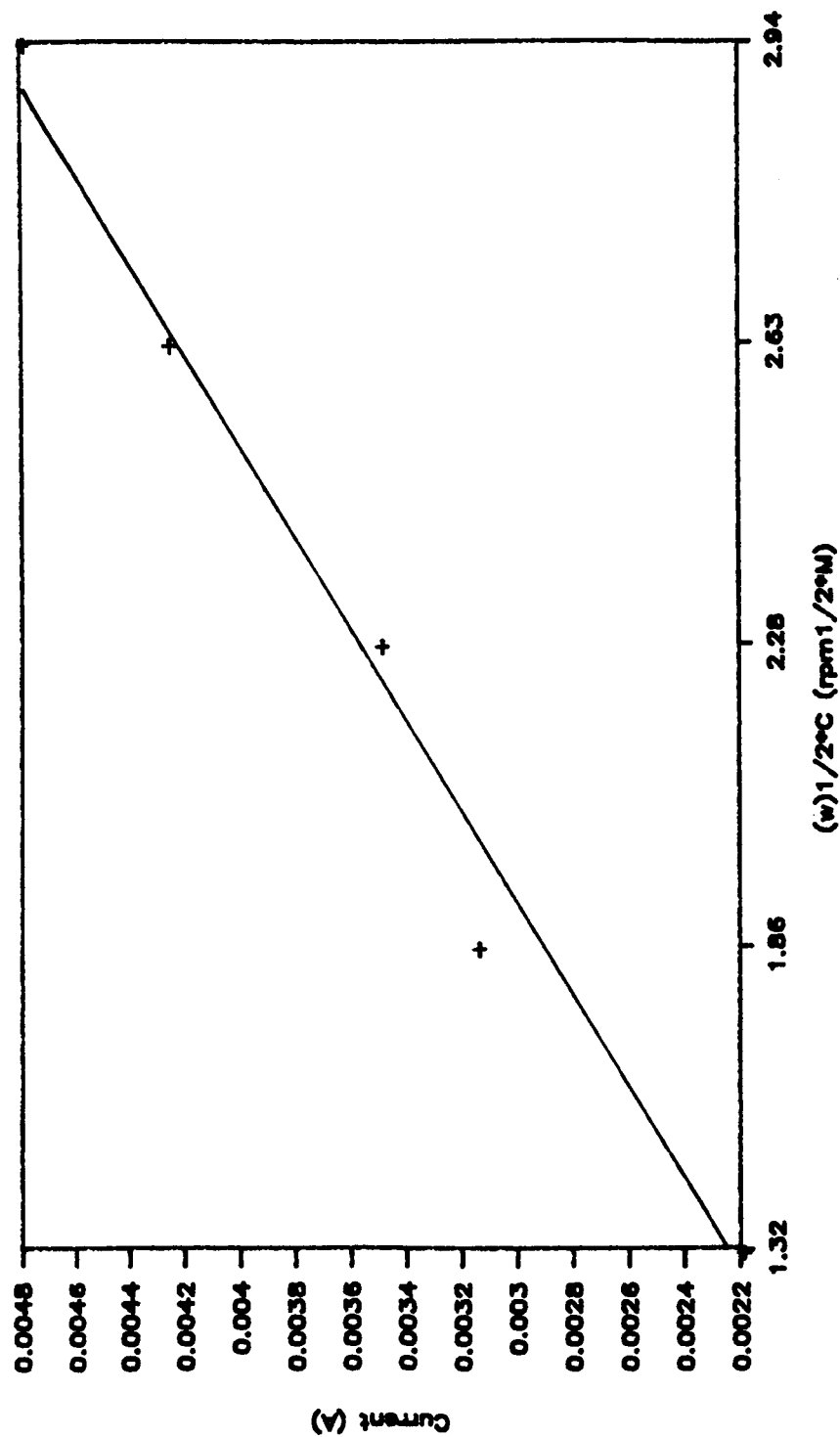
$(w)1/2$°C $(rpm1/2°W)$

Figure 10: Limiting current versus rotation speed for a Au RDE in the presence of 5 ml of 1.38 M H_2O_2 and 50 ml of 31% KOH at 25 °C.
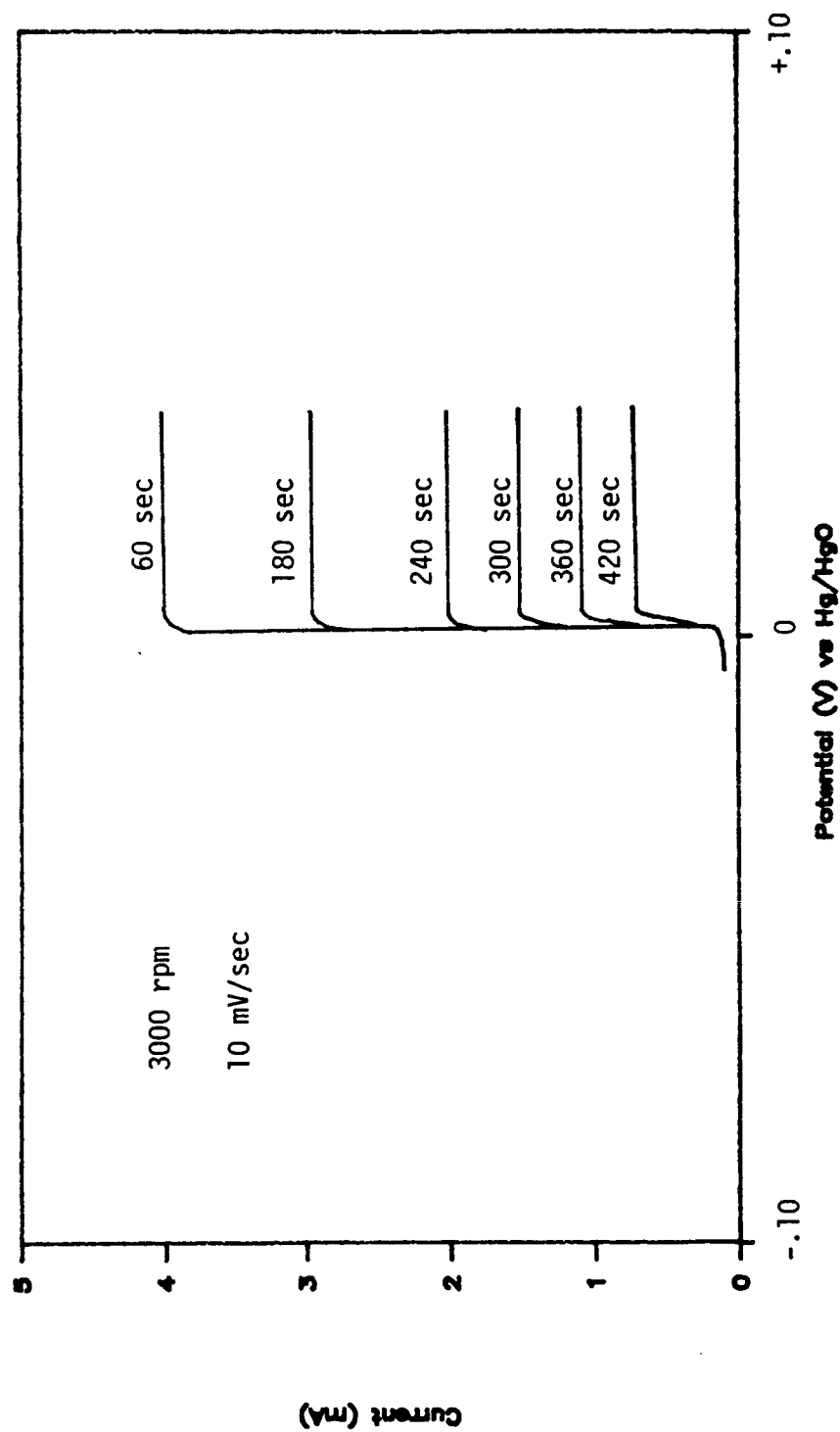
RDE DATA FOR PLATINUM

3000 rpm

10 mV/sec

60 sec

180 sec

240 sec

300 sec

360 sec

420 sec

Current (mA)

Potential (V) vs Hg/HgO

−.10   0   +.10

0   1   2   3   4   5

Figure 11A: RDE data for 50 mg of Pt powder in 31% KOH at 25 $^{\circ}$C.

RDE PLOT FOR PT POWDER

$C_0(HO_2^-) = .126$ M

Time (seconds)

ln(C/Co)

124   184   245   303   364   423   484   544   604

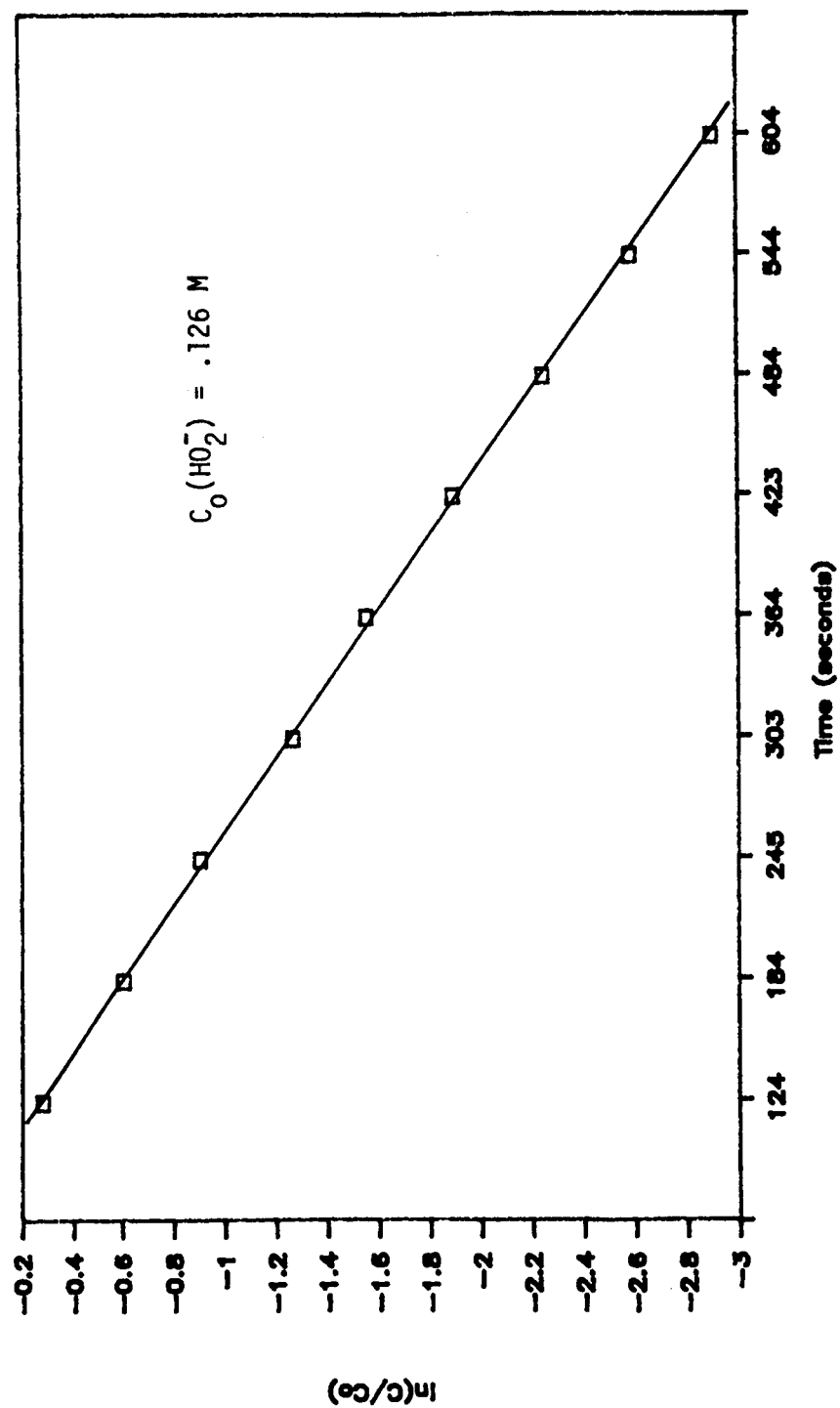-0.2 -0.4 -0.6 -0.8 -1 -1.2 -1.4 -1.6 -1.8 -2 -2.2 -2.4 -2.6 -2.8 -3

Figure 11B: RDE plot for 50 mg of Pt powder in 31% KOH at 25 ^{o}C.

50

5. OPEN CIRCUIT POTENTIAL DECAY STUDIES

Open circuit potential decay studies have shown that HO_2^- decomposition after current interruption is pseudo-second order for all electrodes studied with the exception of $La_{.5}Pb_{.5}MnO_3$. Thus it was necessary to plot $1/C - 1/C_0$ versus time in order to obtain k_h. Results of OCPD studies of the EMC platinum electrode are given in Figures 12A and 12B. For the $La_{.5}Pb_{.5}MnO_3$ electrode, the decomposition was first order and a plot of $\ln(C/C_0)$ versus time was used to obtain k_h. These results are given in Figures 13A and 13B. At polarizing currents above two milliamps, reliable data could not be obtained, therefore all potential decay curves were obtained using polarizing currents of less than two milliamps. The results of the OCPD measurements of the six electrodes are summarized in Table 5. All rate constants have been normalized to unit catalyst surface area and are given in units of cm/s. All experiments were conducted in 31% KOH at 25 $^{\circ}$C.

6. STEADY-STATE POLARIZATION STUDIES

Steady-state polarizations were obtained in the region between 10 and 100 mA cathodic. The data was corrected for ohmic polarization, and Tafel plots were constructed from
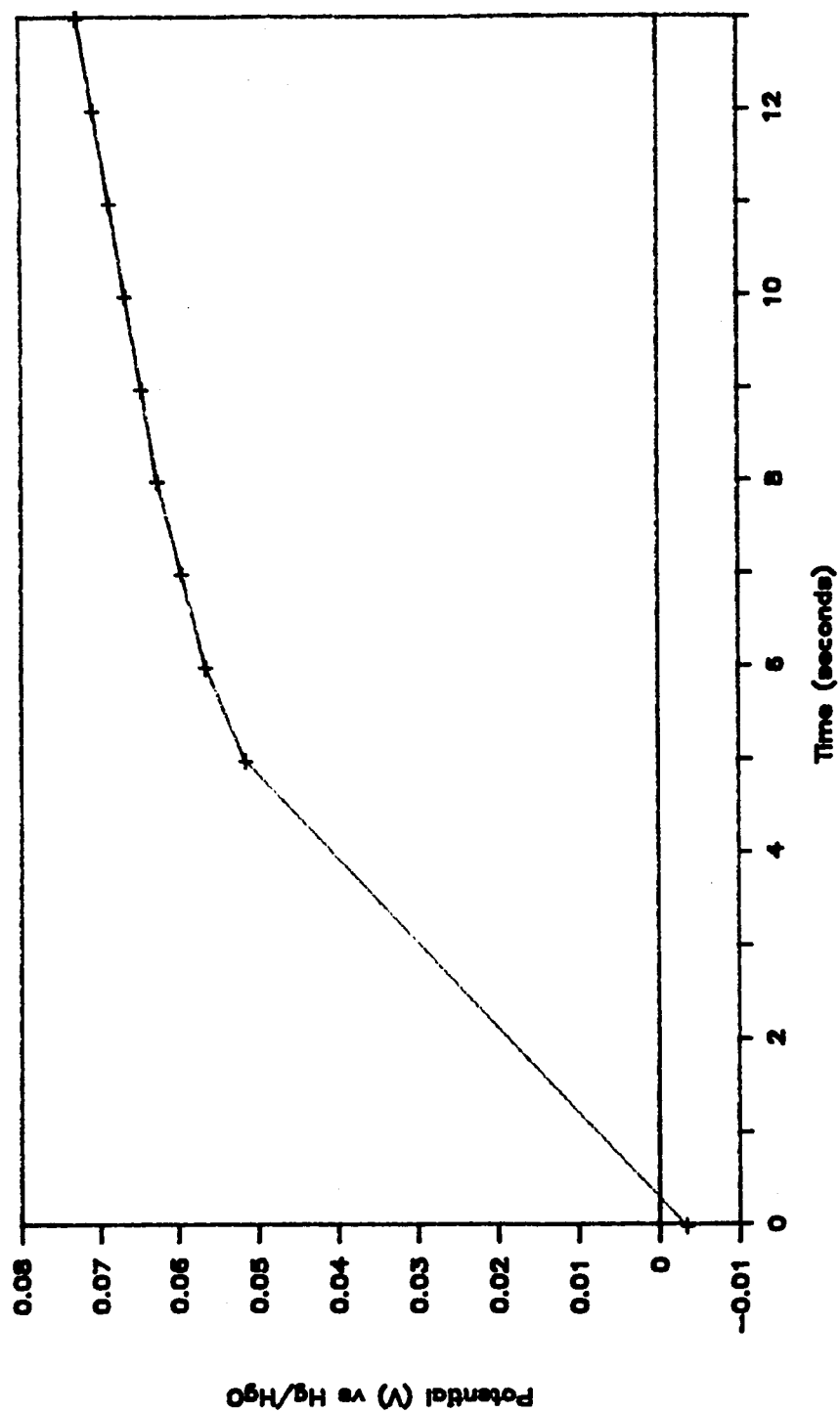
51

OCPD DATA FOR EMC PT

Figure 12A: OCPD data for EMC Pt electrode with .5 mA applied current in 31% KOH at 25 °C.
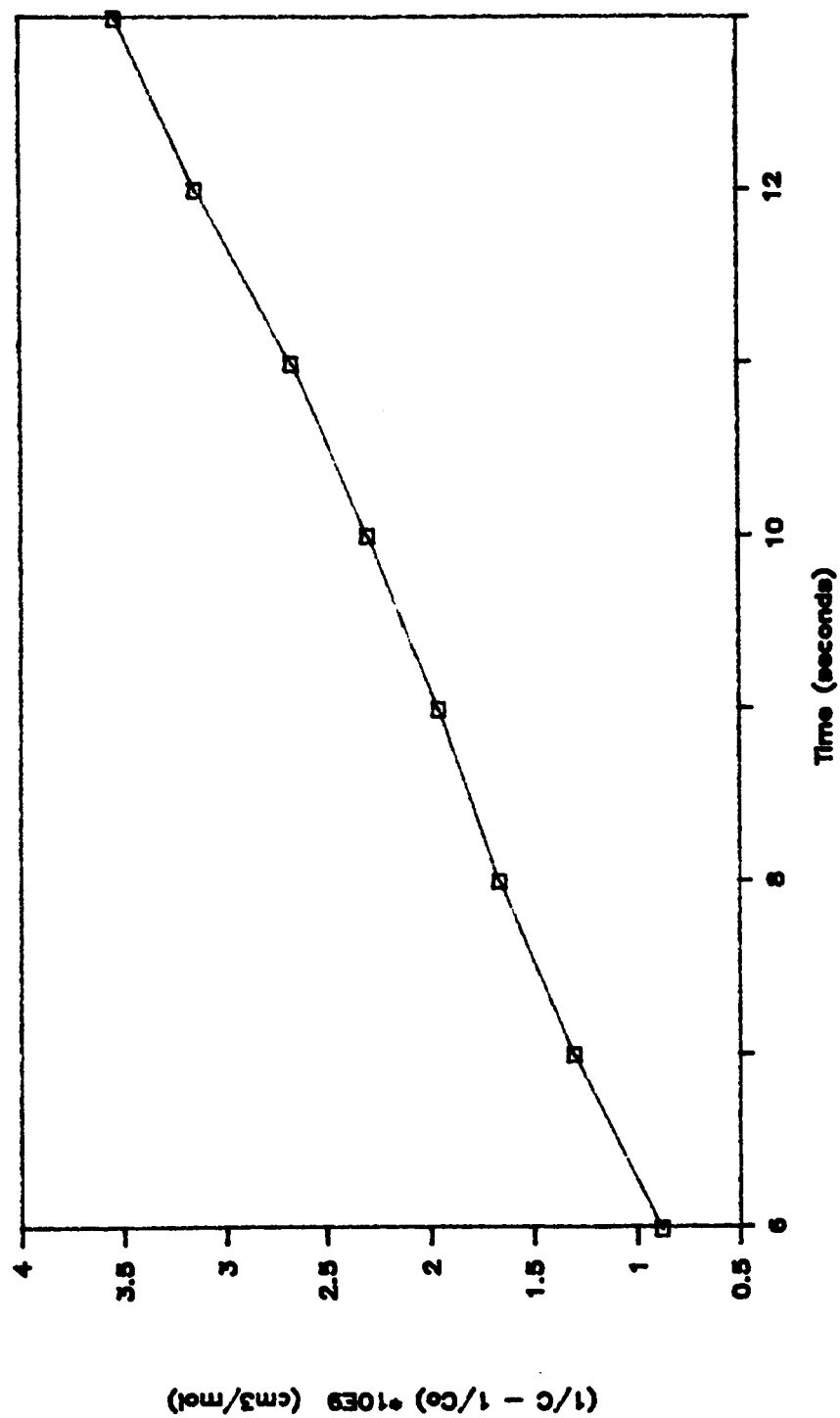
OCPD PLOT FOR EMC PT

Figure 12B: OCPD plot for EMC Pt electrode with .5 mA applied current in 31% KOH at 25 °C.
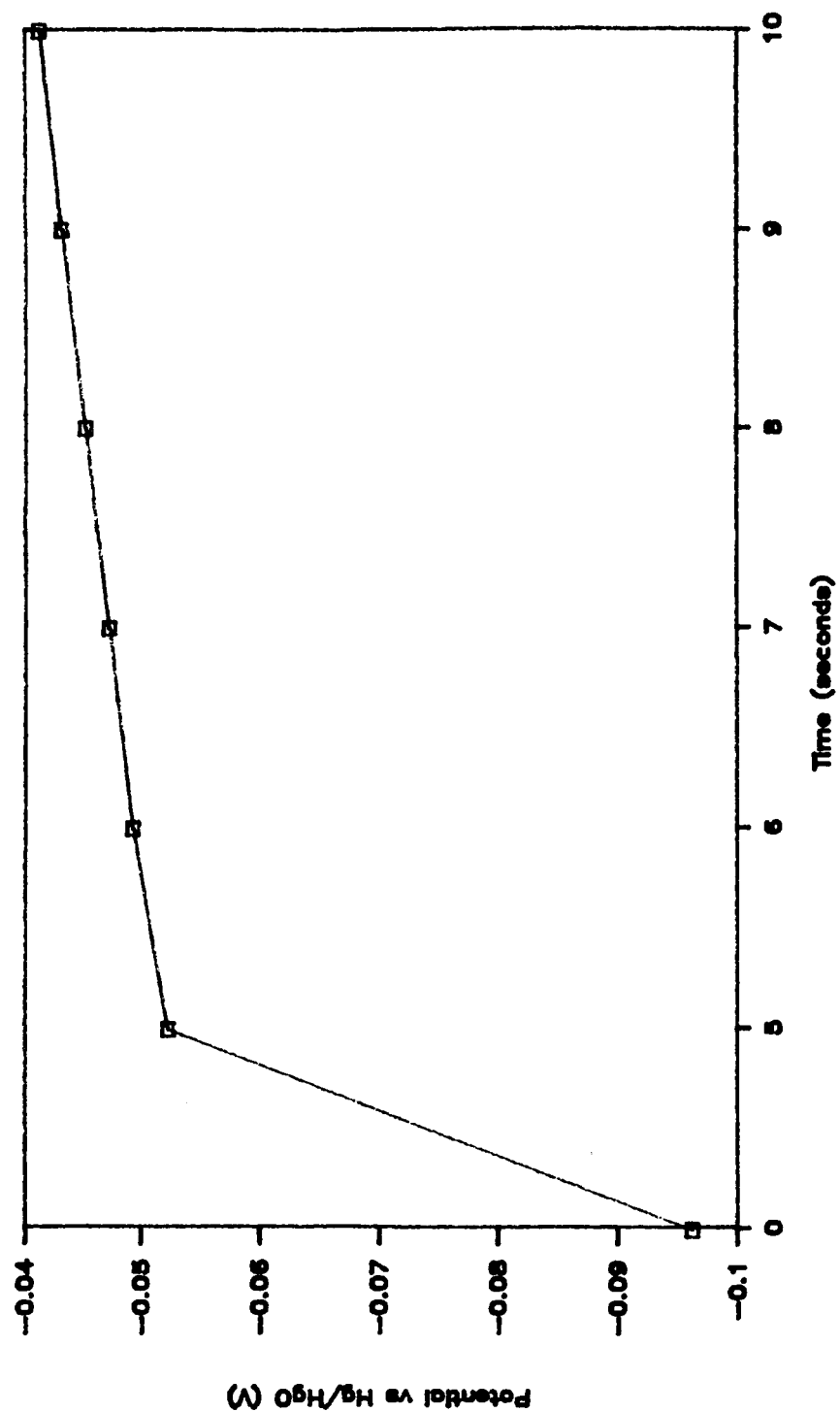
53

OCPD DATA FOR La.5Pb.5MnO3

Potential vs Hg/HgO (V)

Time (seconds)

Figure 13A: OCPD data for $La_{.5}Pb_{.5}MnO_3$ electrode for .5 mA applied current in 31% KOH at 25 ^{o}C.
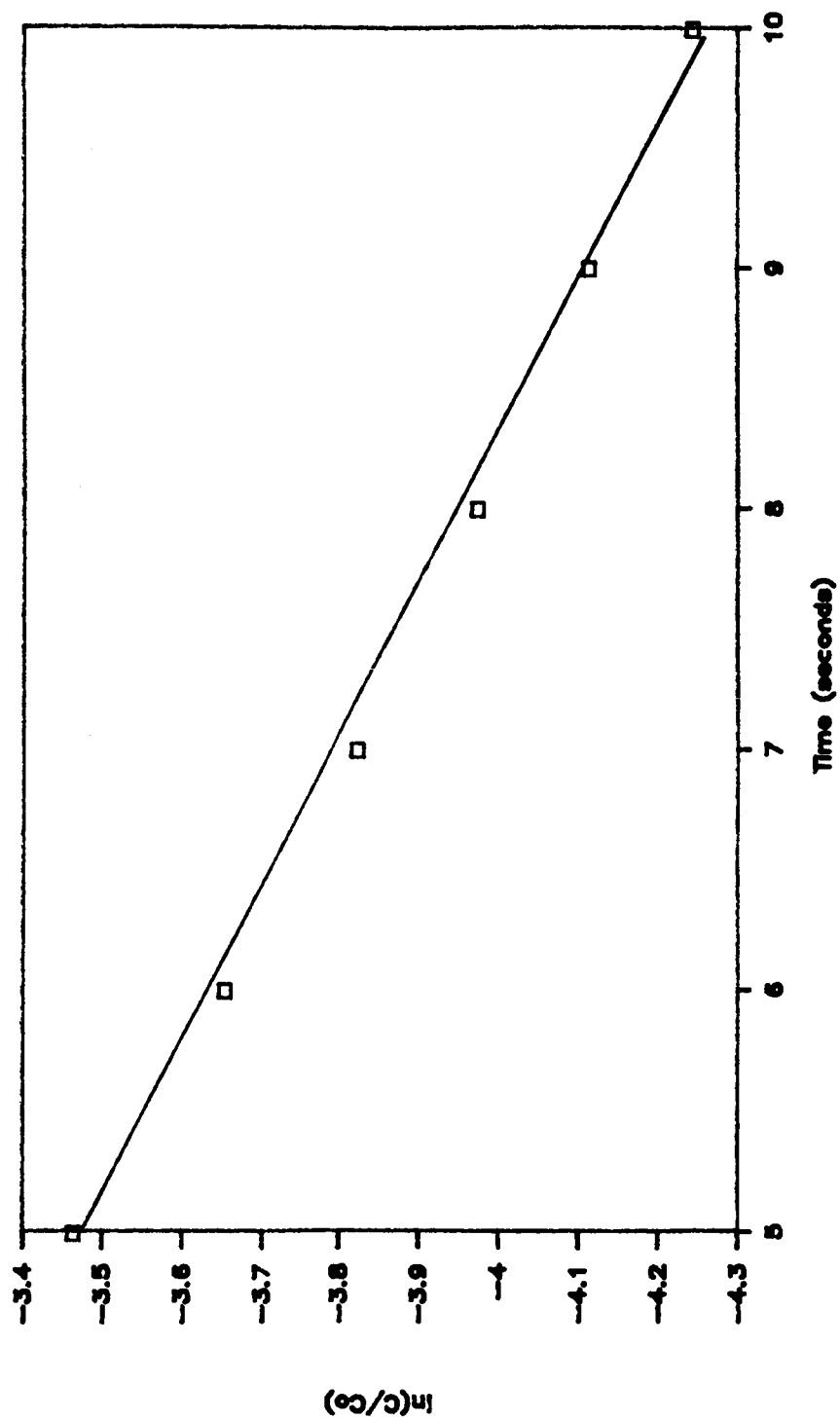
54

OCPD PLOT FOR La.5Pb.5MnO3

Figure 13B: OCPD plot for La$_{.5}$Pb$_{.5}$MnO$_3$ electrode for .5 mA applied current in 31% KOH at 25 ^{o}C.

Table 5: First order rate constants (cm/s) and Tafel slopes (mV/decade) for the six electrodes as determined by open circuit potential decay and steady-state polarization measurements in 31% KOH at 25 °C.

Electrode #	Description	OCPD Studies	SSP Studies	Tafel Slope
1	5 mg Pt on XC72 (EMC)	9.7×10^{-5}	1.3×10^{-5}	-60
2	7 mg Pt "un-supported" (Hughes)	1.7×10^{-3}	3.4×10^{-5}	-49
3	.5 mg Au on acetylene black(Elec-trochem)	2.0×10^{-6}	1×10^{-15}	-268[a]
4	20 mg Au,10% Pt "unsup-ported(IFC)	7.3×10^{-5}	9.1×10^{-7}	-68
5	CoTMPP cat-alyzed car-bon black (EMC)	1.2×10^{-6}	3.2×10^{-7}	-47
6	$La_{.5}Pb_{.5}MnO_3$ 1.3 mg on acetylene black (ELTECH)	7.6×10^{-6}	8×10^{-22}	-310[a]

[a] not a true Tafel slope

this data using equation (12). A Tafel plot for the EMC platinum electrode is given in Figure 14. Data from the Tafel-linear region was used to calculate k_h using equation (13). Results of steady-state polarization measurements of the EMC platinum electrode are given in Figures 15A and 15B. Tafel slopes and decomposition rate constants for the six electrodes determined by SSP are summarized in Table 5.

IV. DISCUSSION

It is convenient to express the heterogeneous rate constants in a form normalized to catalyst surface area. It is therefore important to be able to determine the true active surface area of the catalysts. This is not a difficult task when using catalyst powders, however, the presence of carbon in many of the Teflon-bonded electrodes interferes with the accurate determination of true catalytic surface areas.

One way to determine catalyst surface area is by low temperature N_2 gas adsorption (BET) [33]. BET is one of the most frequently used techniques and usually yields reliable results, provided that the sample size is large enough to insure that the measured surface area is greater than 0.20 m^2. It has been argued that the area determined
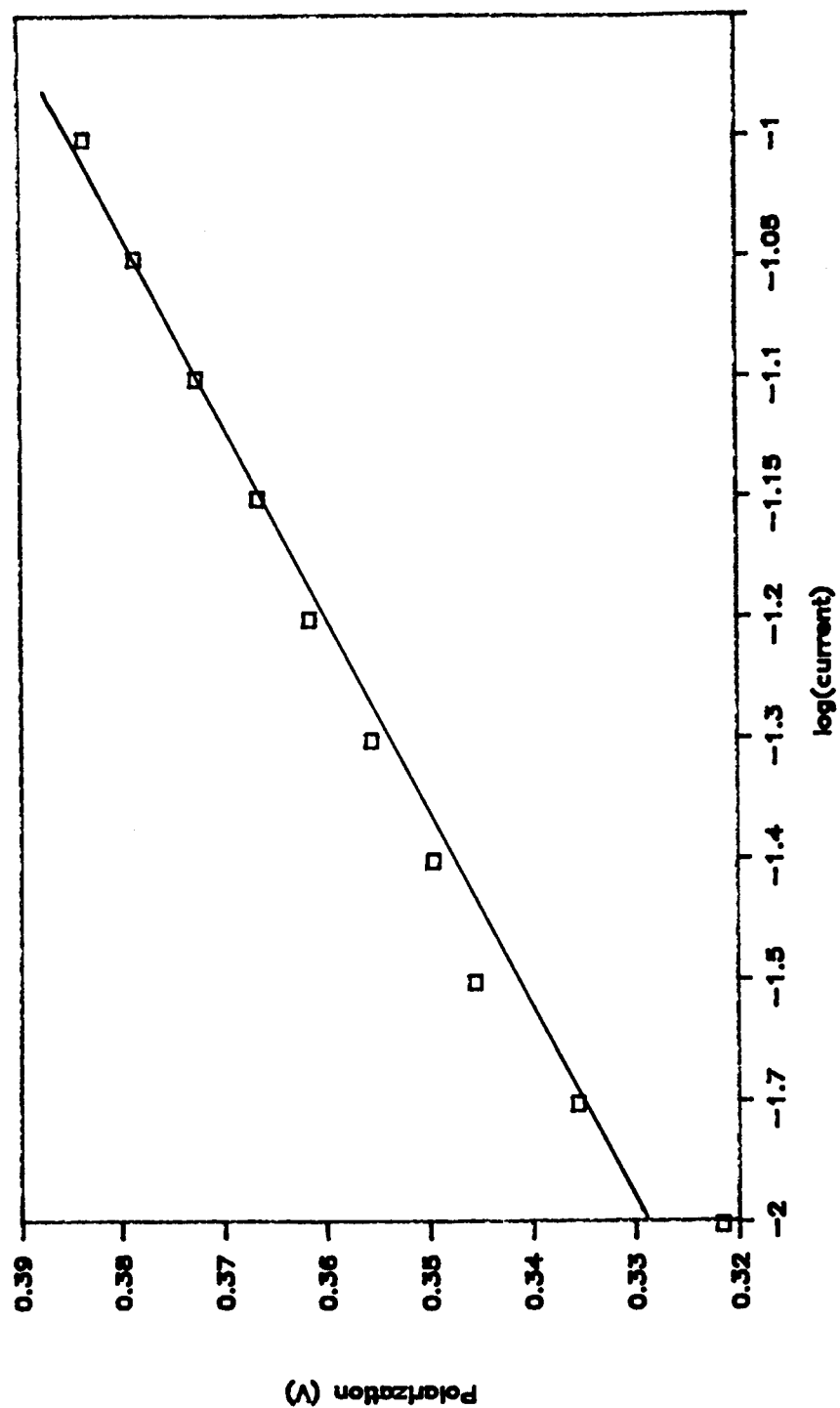
Figure 14: Tafel plot for the EMC electrode in 31% KOH at 25 °C.

SSP DATA FOR EMC PT

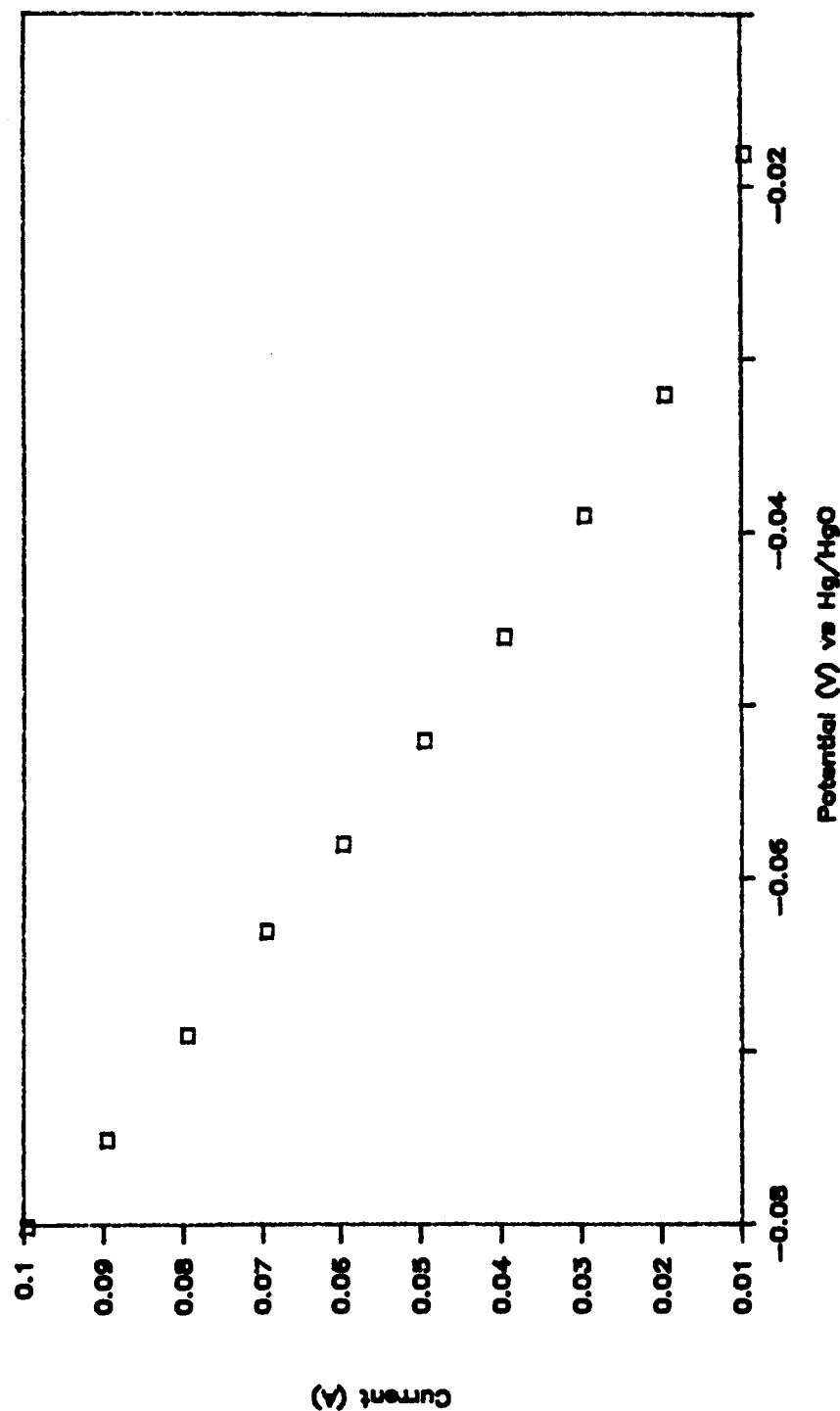Figure 15A: SSP data for the EMC Pt electrode in 31% KOH at 25 $^{\circ}$C.
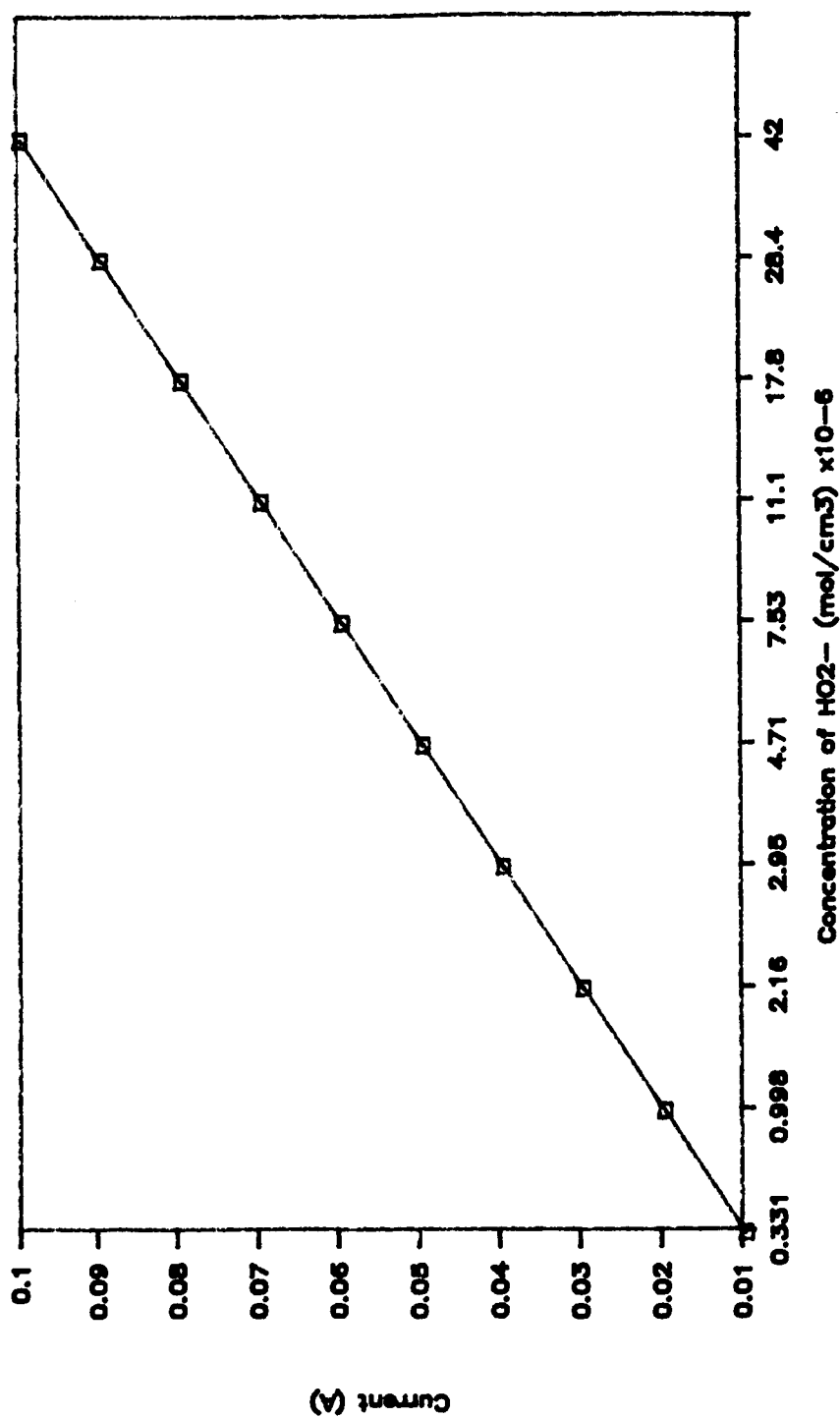
Figure 15B: SSP plot for the EMC Pt electrode in 31% KOH at 25 °C.

by BET may be higher than the surface area associated with electrochemical processes, as the inside surfaces of many pores are not effective in, or contribute but slightly to, the transfer of charge in an electrochemical process [34]. Also, blocking of the pores of transition metal oxides by adsorbed H_2O and OH species will prevent N_2 adsorption and can lead to erroneous results. Removal of these species, even under vacuum conditions, requires temperatures high enough to cause sintering [50]. In addition, BET measures only total surface area, and, when high surface area carbons (50-1400 m^2/g) are added to the electrodes, BET measurements of catalyst surface area become erroneously large. For example, BET measurements of the EMC platinum on XC-72 carbon electrode yielded a surface area which was an order of magnitude greater than the platinum surface area as determined by H_2 adsorption. However, in the case of the heat treated macrocycles like CoTMPP, it is probable that both oxygen reduction and hydrogen peroxide decomposition take place on the same modified carbon surface [31], therefore the active surface area is the total area of the powder or electrode, carbon included.

Hydrogen adsorption is a fairly reliable alternative to BET for measuring surface areas of the platinum electrodes [37,38]. However, it is difficult to separate the charge associated with the adsorption of hydrogen atoms from the charge associated with the simultaneous faradaic reaction, the evolution of hydrogen [52]. Also, it should be noted

that in converting charge to surface area, the most common factors, 210 and 240 microfarads per cm^2, represent a difference of 13% [37]. In addition, for electrodes which contain carbon, it has been reported [35] that hydrogen spillover onto the carbon support is a problem, and leads to erroneously large surface areas. Hydrogen spillover may be occurring to some extent on the EMC platinum electrode as the surface area measured by hydrogen adsorption was about two times higher than the calculated surface area.

Capacitance measurements have been used to determine active surface areas of many metals [34,35] and some metal oxides [51]. However, before calculations can be carried out, the value of the capacitance per unit surface area of the catalyst must be known. The capacitance per unit surface area for the platinum disk in this work was determined to be 128 microfarads per cm^2. This value is close to a reported value of 115 microfarads per cm^2 [65]. The capacitance per cm^2 for the gold disk in this work was found to be 125 microfarads. This value is higher than a reported value of 96 microfarads per cm^2 [53]. It is probable that the roughness factor for the gold disk was greater than two, leading to a high value for the capacitance per cm^2. It should be noted that the capacitance may depend on surface roughness, and the use of a capacitance of a smooth electrode for surface area measurements of Teflon-bonded electrodes may lead to anomalous results as the capacitance in narrow pores is high

in comparison to the capacitance of a smooth surface [34]. Also, care must be taken to insure that no background faradaic processes interfere with the determination of electrode capacitances. In addition, it has been found that the results obtained depend on the frequency of the applied signal [54,55].

It is also possible to determine electrode surface areas from calculations based on catalyst surface area and electrode loading. These calculations are based on the assumption that the catalyst surface is 100 per cent utilized. Surface area measurements for the Hughes platinum electrode, based on calculations, hydrogen adsorption, and capacitance measurements, differed by less than 10% (see Table 3). BET surface area measurements of the IFC gold electrode were within 2% of the value calculated from electrode loading and catalyst powder surface area. For the CoTMPP electrode, the BET surface area was only 50% of the calculated value. Therefore, it appears that catalyst availability is dependent on fabrication parameters such as catalyst loading, firing times, and firing temperatures. However, when properly fabricated, electrodes can have catalyst surface availabilities which approach 100%. The powder surface areas used in the calculations are determined by BET or SEM. When using SEM, one must assume that the particles are spherical in order to calculate a surface area. Also, SEM measurements ignore the porous structure of the catalyst particles. As a result, SEM will only give a

rough estimate of the true catalyst surface area.

The rate constants determined by oxygen probe and gasometric studies differed by only 5% for all of the catalyst powders studied (see Table 4). The RDE studies yielded rate constants which were in agreement with the rate constants determined by oxygen probe and gasometric studies, with the exception of the CoTMPP powder. For the CoTMPP powder, the rate constant determined by RDE studies was 70% higher than the rate constant determined by oxygen probe studies. This value is higher than expected, and may be attributed to an increase in the wetting of the CoTMPP powder for the RDE experiment. Of the three methods, RDE studies are probably the most reliable. RDE experiments monitor the concentration of HO_2^- directly and are sensitive to small changes in the HO_2^- concentration. Both the oxygen probe and gasometric studies monitor the rate of production of oxygen gas which is formed as a reaction product. These measurements are complicated by oxygen leakage into the system for oxygen probe studies, and oxygen leakage out of the system for gasometric studies. Also, both methods are insensitive to small changes in HO_2^- concentration. However, despite these drawbacks, oxygen probe and gasometric studies still yield results which are comparable to those obtained by RDE studies. Of the three methods, the oxygen probe studies are by far the most easily conducted. The gasometric studies require a carefully sealed system, and the gas buret should ideally be

64

encased in a water jacket to insure thermal equilibrium between the solution and the oxygen gas. These are not requirements for the oxygen probe studies. Also, the gasometric studies require constant monitoring of the oxygen volume by the operator during the entire course of the reaction. The use of a recorder in the oxygen probe studies frees the operator from this task. RDE studies require constant interaction between the operator and the instrument to insure that the potential scan is properly timed.

Open circuit potential decay studies of the EMC platinum electrode yielded a rate constant which differed by only 10% from the rate constants determined by RDE, oxygen probe, and gasometric studies (see Table 5). However, OCPD studies of the Hughes platinum electrode yielded a rate constant which was about sixteen times greater than the rate constants determined by RDE, oxygen probe, and gasometric studies. This discrepancy may be due to the fact that the EMC platinum electrode contains carbon whereas the Hughes platinum electrode does not. The presence of carbon is important as it insures the reversibility of the two electron reduction of oxygen [31]. Since the derivation of equation (11) is based on the assumption that the reaction is reversible (see Appendix), it may not be applicable to electrodes without carbon support.

A similar trend holds for the gold electrodes. The Electrochem gold electrode contains carbon, and the rate constant measured by OCPD studies was about one fourth of

the rate constants determined by RDE, oxygen probe, and gasometric studies. The IFC gold electrode does not contain carbon, and the rate constant measured by OCPD studies was about ten times higher than the rate constants measured by RDE, oxygen probe, and gasometric studies.

OCPD studies of the CoTMPP electrode yielded a rate constant that was about 25% less than the rate constants measured by RDE, oxygen probe, and gasometric studies. This difference may be due to incomplete wetting of the electrode pores by the KOH. If the entire surface of the electrode is not wetted, the non-wetted portion of the catalyst will be rendered inactive, resulting in a rate constant which is smaller than is expected.

OCPD studies of the $La_{.5}Pb_{.5}MnO_3$ electrode yielded a rate constant which was about 50% less than the rate constants measured by RDE, oxygen probe, and gasometric studies. Once again the difference may be due to incomplete wetting. Also, for the $La_{.5}Pb_{.5}MnO_3$ electrode, it has been assumed that all of the catalyst powder in the electrode is accessible. This is probably not true, and will lead to a rate constant which is smaller than is expected.

Open circuit potential decay studies are a reliable alternative to RDE, gasometric, and oxygen probe studies for measuring HO_2^- decomposition rate constants provided the electrode contains carbon and the true active surface area of the electrode is known. Also, the experimental apparatus

used for OCPD studies can be used for polarization and corrosion measurements. These measurements are useful for evaluating catalysts for use in fuel cell cathodes. In addition, experimental conditions encountered in the floating half-cell approach the operating conditions in the actual fuel cell.

Steady-state polarization measurements of the six electrodes yielded Tafel slopes which ranged from -47 mV per decade for the CoTMPP electrode, to -68 mV per decade for the IFC gold/platinum electrode. These values are higher than the expected Tafel slope of -29.6 mV per decade for an electrode on which HO_2^- decomposition is the rate limiting step. SSP measurements yielded rate constants which were reasonable for the electrodes with the smallest Tafel slopes. The CoTMPP electrode had a Tafel slope of -47 mV per decade, and SSP measurements yielded a rate constant which was about four times less than the rate constants as determined by RDE, oxygen probe, and gasometric studies. The Hughes platinum electrode had a Tafel slope of -49 mV per decade, and the rate constant measured by SSP was about three times less than the rate constants measured by RDE, oxygen probe and gasometric studies. However, as the deviation between the expected and measured Tafel slope becomes larger, the difference between the expected rate constant and the measured rate constant increases. The Tafel slope of the EMC platinum electrode was -60 mV per decade, and SSP measurements yielded a rate constant that

was about seven times less than the rate constants measured
by RDE, oxygen probe, and gasometric studies. The IFC
gold/platinum electrode had a Tafel slope of -68 mV per
decade, and the rate constant determined by SSP measurements
was about one ninth of the rate constants measured by RDE,
oxygen probe and gasometric studies. The slope of the Tafel
plot of the Electrochem gold electrode was -268 mV per
decade, and the rate constant as determined by SSP
measurements was ten orders of magnitude smaller than
expected. The slope of the Tafel plot of the
$La_{.5}Pb_{.5}MnO_3$ electrode was -310 mV per decade, and SSP
measurements yielded a rate constant which was seventeen
orders of magnitude smaller than the rate constants as
determined by RDE, oxygen probe and gasometric studies. The
slopes of the Tafel plots for the Electrochem gold and
$La_{.5}Pb_{.5}MnO_3$ electrodes imply that mass transport is
rate limiting. The poor performance of the Electrochem gold
and $La_{.5}Pb_{.5}MnO_3$ electrodes may have been the result
of improper electrode fabrication. It is obvious from the
Tafel slopes that HO_2^- decomposition is not the rate
limiting step under the conditions cited for any of the
electrodes studied. Other processes like electron transfer
are probably rate limiting in the current region between 10
and 100 milliamps cathodic. It may be possible to find a
region below 10 milliamps in which HO_2^- decomposition is
the rate limiting step. For example, a Tafel plot of the
EMC platinum electrode in the region between one and ten

68

milliamps gave a Tafel slope of -31 mV per decade. SSP measurements of the EMC electrode in the same current region yielded a rate constant of $(6.3) \times 10^{-5}$ cm/s which compares favorably with the value of $(9.8) \times 10^{-5}$ cm/s measured by RDE studies. However, in practice the interpretation of the cathodic polarization curves at low current densities may be complicated by residual carbon oxidation currents [40].

Platinum is one of the best HO_2^- decomposers known, and has the highest activity of the four catalysts surveyed. In the absence of impurities platinum reduces oxygen primarily by way of the direct four electron reduction to OH^- [9,10,14]. As a result, platinum has been used extensively as the cathode in hydrogen-oxygen fuel cells. One of the major problems which prevents the widespread use of fuel cells is the loss of surface area of the supported platinum black catalyst with time. This loss has been attributed to the gradual dissolution of platinum from the cathode and redeposition in the electrolyte containing matrix [56]. Attempts have been made to solve this problem by using sintering inhibitors or high surface area catalyst supports [57]. However, these efforts have been only partially successful.

The measured activity of gold powder for HO_2^- decomposition is about an order of magnitude less than the activity of platinum. It has been reported that in an alkaline solution the major path for oxygen reduction on gold is the two electron reduction to HO_2^- [22,58].

69

However, work at P&WA's fuel cell facility demonstrated that gold is an excellent catalyst for oxygen reduction and is at least the equal of platinum [56]. These claims would seem contradictory as good performance is usually associated with a high affinity for the direct four electron reduction and HO_2^- decomposition [28]. However, McIntyre and Peck [59] have reported that at pH 14 the electrocatalytic activity of the gold (100) face for oxygen reduction exceeds that of reduced platinum. Gold microcrystallites may present (100) faces at the edges, and may contain surface defects which could act as active sites [60]. Also, gold is not oxidized at cathodic potentials and thus would not be dissolved and transported from the cathode like platinum [56]. These findings may explain the high activity of gold for oxygen reduction.

CoTMPP is approximately fifty times less active than platinum for HO_2^- decomposition, but has a surface area which is about twelve times larger than platinum. In an alkaline solution, the major pathway for reduction of oxygen on CoTMPP is the two electron reduction to HO_2^- [24]. However, it has been reported that in alkaline electrolyte, polarization curves of a heat treated CoTMPP gas-fed cathode are better than those obtained with .5 mg/cm^2 of highly dispersed platinum [9]. Despite encouraging results, stability problems have prevented the use of transition metal macrocyclics in practical cathodes. Instability may be the result of loss of the transition metal from the

complex, degradation of the macrocyclic ligand, or desorption of the macrocyclic complex into the solution [9]. Several groups have reported that heat treatment of transition metal macrocyclics results in considerable gains in stability without losses in activity [61]. The increased stability has been attributed to binding of the reactive part of the ligand to carbon, which prevents oxidative attack [50].

$La_{.5}Pb_{.5}MnO_3$ is only about five times less active than platinum for decomposition of HO_2^-. In addition to high activity for HO_2^- decomposition, many of the perovskites have a high affinity for the four electron reduction of oxygen [28,62]. Also, many perovskites are stable in alkaline medium and have high conductivity [63]. As a result, perovskites have been intensely studied as oxygen reduction electrocatalysts [63-66].

Carbon is often added to the Teflon-bonded electrodes to increase conductivity, prevent catalyst agglomeration, and to insure reversibility of the two electron reduction of oxygen. However, during long term operation the carbon surface is oxidized, resulting in a decrease in electrode performance. Attempts have been made to chemically pretreat the carbon surface in order to achieve greater stability. An interesting alternative to the use of carbon supports is the addition of a stable conducting oxide in place of the carbon. Carbons with a high mineral or ash content also catalyze the decomposition of HO_2^-. However, the

carbons used in this study are not expected to contribute appreciably to the decomposition of HO_2^-.

V. CONCLUSIONS

Surface area measurements by BET yielded reasonable results in the absence of carbon. When carbon was added to the Teflon-bonded electrodes, BET measurements of the active catalyst surface area became erroneously large. A similar trend applied to surface area measurements by double layer capacitance. Hydrogen adsorption measurements worked well for the platinum electrodes without carbon, but hydrogen spillover onto the carbon support may have interfered with the determination of platinum surface area of the EMC electrode. Surface areas were also determined from calculations based on catalyst surface area and electrode loading.

Gasometric, oxygen probe, and RDE studies yielded rate constants which were comparable for the four catalysts surveyed. Of the three methods, RDE studies probably gave the most reliable results. However, gasometric and oxygen probe studies also yielded fairly reliable results and do not require expensive equipment. Oxygen probe studies are the most convenient as they require little interaction between the operator and the instrument.

Open-circuit potential decay measurements can be used to determine HO_2^- decomposition rate constants on Teflon-bonded electrodes provided that the electrode contains carbon. The presence of carbon insures the

reversibility of the two electron reduction of oxygen, which is an underlying assumption in the derivation of equation (11). When carbon is absent, equation (11) may not be valid, and the resulting rate constants become erroneously large. It is also important to be able to accurately determine the true active surface area of the catalyst in the Teflon-bonded electrodes. Surface area measurements are complicated by the presence of carbon, and uncertainties in the catalytic surface area can lead to large errors in the value of the decomposition rate constant.

Measurements of HO_2^- decomposition rate constants by steady-state polarization have been only marginally successful. SSP measurements yielded rate constants which were reasonable for the electrodes whose Tafel slopes approached the expected value of -29.6 mV per decade. However, when the Tafel slopes deviated appreciably from the expected value, the error of the measured rate constants became extremely large.

Each of the above mentioned methods can be used to measure HO_2^- decomposition rate constants provided that precautions are taken to insure the validity of the assumptions used in the derivation of the equations used herein. For OCPD studies, it is important that carbon is included in the Teflon-bonded electrodes to insure the reversibility of the two electron reduction of oxygen. For SSP studies, it is important that the measured Tafel slope of the Teflon-bonded electrode approaches the expected value of -29.6 mV per decade. 74

REFERENCES

1. Grove, W. R., Phil. Mag., $\underline{14}$, 127(1839).

2. Williams, K. R., An Introduction to Fuel Cells, Elsevier Publishing Company, London, 1966.

3. Mond, L., and Langer, C., Proc. Roy Soc., $\underline{46}$, 296(1889).

4. Siegl, K., Elektrotech. Z., $\underline{34}$, 1317(1913).

5. Bacon, F. T., Chapter 5 in Fuel Cells, Vol. 1, Reinhold, New York, 1960.

6. Carnot, S., Reflections of Motive Power of Heat, Am. Soc. Mech. Eng., 1953.

7. Stedman, J. K., 1985 Fuel Cell Seminar Abstracts, pg.138, Sponsored by National Fuel Cell Coordinating Group, Tucson, Arizona, May 19-22(1985).

8. Martin, R. E., "Advanced Technology Lightweight Fuel Cell Program, Final Report", United Technology Corp., Power Systems Division FCR-3045, NASA CR-165417, Aug.79-Feb.81.

9. Yeager, E., "Oxygen Cathodes: Present Status and Problem Areas", Workshop on Renewable Fuels and Advanced Power Sources for Transportation, Boulder,Colorado, June 17-18,1982.

10. Damjanovic, A., Genshaw, M. A. and Bockris, J. O'M., J. Electrochem. Soc., $\underline{114}$, 446(1967).

11. Damjanovic, A., Dey, A., and Bockris, J. O'M., J. Electrochem. Soc., $\underline{113}$, 739(1966).

12. Radyushkina, K. A., Tarasevich, M. R., and Burnstein, R. K., Elektrokhim., $\underline{6}$, 1352(1970).

13. Tarasevich, M. R., Elektrokhim., $\underline{9}$, 599(1973).

14. Molla, J. A., Dissertation, Case Western Reserve University, Cleveland, OH., 1983.

15. Riddiford, A. C., Electrochem. Acta, $\underline{4}$, 170(1961).

16. Muller, L., and Nekrasov, L. N., Electrochim. Acta., $\underline{9}$, 1015(1964).

17. Damjanovic, A., Genshaw, M. A., and Bockris, J. O'M, J. Chem Phys., 45, 4057(1966).

18. Wroblowa, H. S., Pan, Y. C., and Razumney, G., J. Electroanal. Chem., 69, 195(1976).

19. Appelby, A. J., and Savy, M., J.Electroanal. Chem., 92, 15(1978).

20. Zurilla, R. W., Sen, R. K. and Yeager, E., J. Electrochem. Soc., 125, 1123(1978).

21. Bagotskii, V. S., Filinovskii, V., and Shumilova, N. A., Elektrokimica, 4, 1247(1968).

22. Zurilla, R. W., Sen, R. K., and Yeager, E., J. Electrochem. Soc., 125, 1103(1978).

23. Kern, D. M. H., J. Am. Chem. Soc., 76, 4208(1954).

24. Molla, J. A., Gupta, S. L., and Yeager, E., ECS Meeting, Detroit, Michigan(1982), Abstract No. 37.

25. Davies, M., Clark, M., Yeager, E., and Hovorka, F., J. Electrochem. Soc., 106, 56(1959).

26. Genshaw, M. A., Doctorate Dissertation, Univ. of Penn., Philadelphia, PA., 1966.

27. Yeager, E., and Kowzawa, A., Combustion and Propulsion, 6th. AGARD Colloquium, Pergamon, Oxford, 1964.

28. Tseung, A. C. C.,J. Electrochem. Soc., 125, 1660(1978).

29. Onuchukwu, A. I., and Mshella, P. B.,J. Chem. Educ. 62,(1985).

30. Goldstein, J. R., and Tseung, A. C. C., J Physical Chem. 76, 3646, (1972).

31. Carbonio, R. E., Tryk, D., and Yeager E., ECS Meeting Spring, 1987.

32. Goldstien, J. R., and Tseung, A. C. C., Journal of Catalysis, 32, 452(1974).

33. Brunauer, S., Emmet, P., and Teller, E., J. Amer. Chem. Soc. 60, 309(1938).

34. Feltham, A. M., and Spiro, M., Chem. Rev., 71, 177(1971).

35. Brodd, R. J., and Hackerman, N., J. Electrochem. Soc., 104, 705(1957).

36. Ives, D., and Janz, G., Reference Electrodes, Academic Press, New York, 1961.

37. Hayes, M., and Kuhn, A. T., Applications of Surface Science, 6, 1(1981).

38. Barna, G. G., Frank, S. N., and Teherani, T. H., J. Electrochem. Soc., 129, 4(1982).

39. Bard A. J., and Faulkner L. R., "Electrochemical Methods, Fundamentals and Applications," John Wiley and Sons, N. Y., (1980), pg. 288.

40. Tryk, D., and Yeager E., ECS Meeting, Oct 17-21, 1982, Volume 82-2, Abstract no. 36.

41. Giner, J., and Smith, S., Electrochem. Technol., 5, 61(1967).

42. Giner, J., Parry, J. M., Smith, S., and Turchan, M., J. Electrochem. Soc., 116, 1692(1969).

43. Vogel, A. I., Vogel's Textbook of Quantitative Inorganic Analysis, Fourth Edition, New York, (1978).

44. Yeager, E., Kozawa, A., Tech. Rep. No. 17, Office of Naval Res., Contract No. 2391(00), 1964.

45. Levich, V. G., Physicochemical Hydrodynamics, Eng. transl. by Scripta Technica, Inc., Prentice Hall, Inc., Englewood Cliffs, NJ, 1962.

46. Pleskov, Yu. V., and Filinovskii, V. Yu., The Rotating Disk Electrode, Eng. transl. by H. S. Wroblowa, Consultant Bureau, New York, 1976.

47. Galasso, F. S., Structure, Properties and Preparation of Perovskite-type Compounds, Pergamon Press, London,1969.

48. Vassie, P. R., and Tseung, A. C. C., Electrochim. Acta, 20, 759(1975).

49. Vassie, P. R., and Tseung, A. C. C., Electrochim. Acta, 20, 762(1975).

50. Scherson, D. A., Gupta, S. L., Fierro, C., and Yeager, E. B., Electrochim. Acta, 28, 1205(1983).

51. Burke, L. D., and Murphy, O. J., J. Electroanal. Chem. 96, 19(1979).

52. Woods, R., J. Electroanal. Chem. Interfacial Electrochem. 49,217(1974).

53. Giner, J., Parry, J., Swette, L., and Cattabriga, R., "Development of Cathodic Electrocatalysts for Use in Low Temperature H_2/O_2 Fuel Cells with Alkaline Electrolyte", Tyco Laboratories Inc., NASW-1233, July 65'-June 67'.

54. Choudhary, G., Trans. Indian Inst. Metals, 24, 1(1971).

55. Cooper, I. L., Harrison, J. A., and Sandbach, D. R., Electrochim. Acta., 23, 527(1978).

56. Freed, M. S., and Lawrance, R. J., ECS Meeting, Toronto (1975).

57. Tseung, A. C. C., and Dhara, S. C., Electrochimica Acta, 20, 681(1985).

58. Strasser, K., J. Electrochem. Soc., 127, 2172(1980).

59. McIntyre, J. D. E., and Peck, W. F., Electrochemistry at Single Crystal Metal Electrodes: Proceedings of the Symposium on the Chemistry and Physics of Electrocatalysis, The Electrochemical Society, Vol. 84-12, 102(1984).

60. Singer, J., and Srinivasan, V., Evaluation Parameters for the Alkaline Fuel Cell Oxygen Electrode, NASA Technical Memorandum 87155.

61. van Veen, J. A., van Baar, J. F., and Kroese, K. J., J. Chem Soc., Faraday Trans. I 77, 2827(1981).

62. Tseung, A. C. C., and Bevan, H. L., J. Electroanal. Chem., 45, 429(1975).

63. Obayashi, H., and Kudo, T., Mat. Res. Bull., 13, 1409(1978).

64. Bronoel, G., Grenier, J. C., and Reby, J., Electrochim. Acta, 25, 1015(1980).

65. Matsumoto, Y., Yoneyama, H., and Tamura, H., Chem. Lett., 661(1975).

66. Matsumoto, Y., and Sato, E., Electrochim. Acta, 25, 585 (1980).

67. Goldstein, J. R., and Tseung, A. C. C., J. Mater. Sci., 7, 1383(1972).

Derivation of Equation (11) [31,40]

The two electron reduction of oxygen (see reaction (2)) is reversible on high surface area carbon, and the Nernst equation for this reaction is given by,

$$E = E_0 - RT/NF \times \ln[a_{HO2}^- x_{OH-}^a / a_{H2O}^a x_{O2}^P] \quad (15)$$

If the following assumptions are valid,

1. The O_2 partial pressure within the electrode must remain at one atmosphere.

2. The HO_2^- concentration is uniform within the wetted portion of the electrode except on the microscopic scale around each catalyst particle.

3. Diffusion of HO_2^- out of the electrode is relatively slow.

4. The potential is not perturbed by the presence of other redox couples.

5. The activity coefficients of HO_2^- and OH^- are equal.

the Nernst equation can be modified:

$$E_t = E' - RT/2F \times \ln(C_{HO_2^-})t + RT/2F \times \ln(P_{O_2}) \quad (16)$$

here the potential at time t, Et, is relative to the Hg/HgO reference electrode and,

$$E' = E_0(O_2/HO_2^-) + E_0(Hg/HgO) + RT/2F \times \ln(C_{OH}^-) \quad (17)$$

$$= -.209 \text{ V vs. Hg/HgO in 31\% KOH at 25 C.}$$

Assuming $PO_2 = 1$,

$$E_t = -.209 \text{ V} - RT/2F \times \ln(CHO_2^-)_t \quad (18).$$

For first order decomposition of HO_2^-,

$$(V_1/A_c) \times (dC/dt) = k_{het} \times C \quad (19).$$

Then,

$$E_t = E' - RT/2F \times \ln(C_{HO2}^-)_0 + RT/2F \times kt \quad (20).$$

As the total capacitance of the electrode discharges, there is a further cathodic production of HO_2^- via equation (2). The discharge current is ,

$$I = Ctot(dE/dt) \quad (21).$$

The rate of appearance of HO_2^- due to this current flow is,

$$(V_1/A_c) \times (dC/dt) = -(I/2FA_c) \quad (22).$$

Substituting equation (21) into equation (22),

$$(V_1/A_c) \times (dC/dt) = (C_t/2FA_c) \times (dE/dt) \quad (23).$$

From the Nernst equation,

$$dE = -[(RT/2F) \times (dC_{HO2}^-/C_{HO2}^-)] \quad (24).$$

Substituting equation (24) into equation (23),

$$(V_1/A_c) \times (dC/dt) = (C_t RT/4F^2 A_c) \times (1/C) \times (dC/dt) \quad (25).$$

Adding equations (19) and (25) and rearranging,

$$(V_1/A_c) \times (dC/dt) - (C_t RT/4F^2 A_c)(1/C)(dC/dt) = -k \times C \quad (26).$$

Multiplying through by dt and dividing by c,

$$(V_1/A_c)(dC/C) - (C_t RT/4F^2 A_c)(dC/C^2) = -kdt \quad (27).$$

After integration,

$$(V_1/A_c)[\ln(C/C_0)] - (RTC_t/4F^2 A_c)[1/C - 1/C_0] = -kt$$

(28),

which is equation (11).

Report Documentation Page

1. Report No. NASA TM-101333	2. Government Accession No.	3. Recipient's Catalog No.
4. Title and Subtitle Electrocatalytic Reduction of Oxygen on Modified Oxide Surfaces		5. Report Date September 1988
		6. Performing Organization Code
7. Author(s) Scott A. Chaffins, Vakula S. Srinivasan, and Joseph Singer		8. Performing Organization Report No. E-4345
		10. Work Unit No. 506-41-21
9. Performing Organization Name and Address National Aeronautics and Space Administration Lewis Research Center Cleveland, Ohio 44135-3191		11. Contract or Grant No.
		13. Type of Report and Period Covered Technical Memorandum
12. Sponsoring Agency Name and Address National Aeronautics and Space Administration Washington, D.C. 20546-0001		14. Sponsoring Agency Code

16. Abstract

A first step which frequently occurs in the reduction of dioxygen, e.g. at the cathode of the alkaline fuel cell, is the two-electron reduction to peroxyl ion, HO_2^-. For efficiency of the fuel cell, this ion must be further reduced, or decomposed, to OH^-. Rate constants for HO_2^- decomposition have been determined in 31 percent KOH at 25 °C for the following catalysts in the form of suspended powders and Teflon-bonded electrodes: Pt, Au, cobalt tetramethoxy phenyl porphyrin (CoTMPP), and $La_{0.5}Pb_{0.5}MnO_3$. Rates were normalized to unit surface area measured by several methods as suitable. Where possible, four methods were used to measure rate constants: gasometric, oxygen probe, rotating disk electrode, and open-circuit potential decay. Steady-state polarization was also tried but was not as satisfactory. Comparisons are given for the methods in regard to reliability, applicability to the material, and convenience.

17. Key Words (Suggested by Author(s)) Oxygen cathode Peroxide decomposition rate constants Teflon-bonded electrodes Perovskites	18. Distribution Statement Unclassified – Unlimited Subject Category 25		
19. Security Classif. (of this report) Unclassified	20. Security Classif. (of this page) Unclassified	21. No of pages 84	22. Price* A05